

ISTANBUL TECHNICAL UNIVERSITY ★ INSTITUTE OF SCIENCE AND TECHNOLOGY

**BAYESIAN COMPRESSIVE SENSING APPROACH
FOR ULTRA-WIDEBAND CHANNEL ESTIMATION**

M.Sc. THESIS

Mehmet ÖZGÖR

Department of Electronics and Communication Engineering

Telecommunication Engineering Programme

JANUARY 2013

**BAYESIAN COMPRESSIVE SENSING APPROACH
FOR ULTRA-WIDEBAND CHANNEL ESTIMATION**

M.Sc. THESIS

**Mehmet ÖZGÖR
(504101316)**

Department of Electronics and Communication Engineering

Telecommunication Engineering Programme

Thesis Advisor: Prof. Dr. Hakan Ali ÇIRPAN

JANUARY 2013

**ULTRA GENİŞ BANT KANAL KESTİRİMİ İÇİN
BAYES SIKIŞTIRILMIŞ ALGILAMA YAKLAŞIMI**

YÜKSEK LİSANS TEZİ

**Mehmet ÖZGÖR
(504101316)**

Elektronik ve Haberleşme Mühendisliği Anabilim Dalı

Telekomünikasyon Mühendisliği Programı

Tez Danışmanı: Prof. Dr. Hakan Ali ÇIRPAN

OCAK 2013

To my family,

FOREWORD

First of all, I would like to express my appreciation to my advisor Prof. Dr. Hakan Ali ÇIRPAN for his invaluable comments and advices during my graduate education. Besides, I would like to express my appreciation to Assist. Prof. Dr. Serhat ERKÜÇÜK for his invaluable guidance and encouragement throughout my research study. I am thankful to my friends for their favorable discussions and constructive suggestions on this thesis.

I would also like to express my profound gratitude to my family due to their precious support and motivation which made this thesis all possible.

Finally, I would like to thank TÜBİTAK (The Scientific and Technological Research Council of Turkey) for providing me scholarship during my M.Sc. study.

January 2013

Mehmet ÖZGÖR
(Electrical and Electronics Engineer)

TABLE OF CONTENTS

| | <u>Page</u> |
|--|-------------|
| FOREWORD | ix |
| TABLE OF CONTENTS | xi |
| ABBREVIATIONS | xiii |
| LIST OF TABLES | xv |
| LIST OF FIGURES | xvii |
| SUMMARY | xix |
| ÖZET | xxi |
| 1. INTRODUCTION | 1 |
| 1.1 Motivation of the Thesis | 1 |
| 1.2 Literature Review | 4 |
| 1.3 Purpose of the Thesis..... | 5 |
| 1.4 Preview of the Thesis..... | 6 |
| 2. ULTRA-WIDEBAND COMMUNICATIONS | 7 |
| 2.1 Overview of Ultra-Wideband Communications | 7 |
| 2.2 Ultra-Wideband Channel Model | 14 |
| 3. COMPRESSIVE SENSING FOR UWB CHANNEL ESTIMATION | 19 |
| 3.1 Overview of Compressive Sensing..... | 19 |
| 3.2 Bayesian Compressive Sensing | 22 |
| 4. PERFORMANCE ANALYSIS | 29 |
| 4.1 MSE of a Biased Estimator | 30 |
| 4.2 MSE of Bayesian Biased Estimator | 30 |
| 5. RESULTS | 35 |
| 5.1 Performance Results | 35 |
| 5.1.1 Effect of number of measurements on the MSE performance | 35 |
| 5.1.2 Effect of channel models on the MSE performance and MSE lower bounds..... | 37 |
| 5.2 Computation Efficiency | 40 |
| 6. CONCLUSION AND FUTURE WORK | 45 |
| REFERENCES | 47 |
| APPENDICES | 53 |
| APPENDIX A: IEEE 802.15.4a UWB Channel Modeling..... | 55 |
| CURRICULUM VITAE | 61 |

ABBREVIATIONS

| | |
|---------------|---|
| A/D | : Analog to Digital |
| AWGN | : Additive White Gaussian Noise |
| BCS | : Bayesian Compressive Sensing |
| BMAP | : Block Maximum A Posteriori |
| BP | : Basis Pursuit |
| BPSK | : Binary Phase Shift Keying |
| BPDN | : Basis Pursuit De-Noising |
| CIR | : Channel Impulse Response |
| CM | : Channel Model |
| CoSaMP | : Compressive Sampling Matching Pursuit |
| CRLB | : Cramér-Rao Lower Bound |
| CPU | : Central Processing Unit |
| CS | : Compressive Sensing |
| dB | : decibel |
| dBm | : decibel-milliwatt |
| EIRP | : Effective Isotropic Radiated Power |
| FCC | : Federal Communications Commission |
| FIM | : Fisher Information Matrix |
| GHz | : Gigahertz |
| GPS | : Global Positioning System |
| IEEE | : Institute of Electrical and Electronics Engineers |
| i.i.d. | : independent identically distributed |
| IR | : Impulse Radio |
| LF | : Likelihood Function |
| LMS | : Least Mean Squares |
| LOS | : Line-of-Sight |
| m | : meter |
| MHz | : Megahertz |
| ML | : Maximum Likelihood |
| MP | : Matching Pursuit |
| MSE | : Mean Square Error |
| NLOS | : Non Line-of-Sight |
| ns | : nanoseconds |
| nW | : nanowatt |
| OMP | : Orthogonal Matching Pursuit |
| PCRLB | : Posterior Cramér-Rao Lower Bound |
| PCS | : Personal Communications Service |
| PPM | : Pulse Position Modulation |
| RAM | : Random Access Memory |
| RF | : Radio Frequency |
| SNR | : Signal-to-Noise Ratio |

StOMP : Stagewise Orthogonal Matching Pursuit
SOCP : Second Order Cone Program
UWB : Ultra-Wideband
WBAN : Wireless Body Area Network
WPAN : Wireless Personal Area Network
WSN : Wireless Sensor Network

LIST OF TABLES

| | <u>Page</u> |
|--|-------------|
| Table 2.1 : Sparsity ratios of channel models when $T_c = 250\text{ns}$ and $T_s = 0.25\text{ns}$. | 18 |
| Table 5.1 : Computation times of both methods for CM-1. | 42 |
| Table 5.2 : Computation times of both methods for CM-2. | 42 |
| Table 5.3 : Computation times of both methods for CM-5. | 42 |
| Table 5.4 : Computation times of both methods for CM-8. | 42 |
| Table 5.5 : Computation times of both methods for channel models when $M = 250$ | 43 |
| Table A.1 : Definitions of the channel parameters given in Table A.2. | 59 |
| Table A.2 : Parameters of the IEEE 802.15.4a UWB channel models used in this thesis [44]. | 60 |

LIST OF FIGURES

| | <u>Page</u> |
|---|-------------|
| Figure 2.1 : FCC spectral mask for indoor UWB communication systems..... | 8 |
| Figure 2.2 : FCC spectral mask for outdoor UWB communication systems..... | 9 |
| Figure 2.3 : Spectrum of UWB and existing narrowband communication systems [41]. | 9 |
| Figure 2.4 : A typical UWB pulse shape..... | 11 |
| Figure 2.5 : An UWB BPSK modulated signal..... | 11 |
| Figure 2.6 : An UWB 4-ary PPM modulated signal. | 12 |
| Figure 2.7 : A transmitted PPM modulated UWB signal..... | 13 |
| Figure 2.8 : The equivalent T_s -spaced channel model example. (a) UWB continuous time CIR; (b) T_s -spaced CIR when $T_s = 1\text{ns}$; (c) T_s -spaced CIR when $T_s = 0.25\text{ns}$ | 15 |
| Figure 2.9 : Realizations of channel models when $T_c = 250\text{ns}$ and $T_s = 0.25\text{ns}$.. | 17 |
| Figure 3.1 : Model of the compressive sensing..... | 20 |
| Figure 3.2 : Estimation of a CM-1 signal with ℓ_1 -norm minimization and BCS when $T_c = 100\text{ns}$, $T_s = 0.25\text{ns}$, $N = 400$, $M = 200$ and $SNR = 5\text{dB}$. (a) A CM-1 signal and its estimation with ℓ_1 -norm minimization, estimation error of the channel coefficients vector for ℓ_1 -norm minimization = 0.4731; (b) Same CM-1 signal in (a) and its estimation with BCS, estimation error of the channel coefficients vector for BCS = 1.0976. | 26 |
| Figure 3.3 : Estimation of the same CM-1 signal in Figure 3.2 with ℓ_1 -norm minimization and BCS when $T_c = 100\text{ns}$, $T_s = 0.25\text{ns}$, $N = 400$, $M = 200$ and $SNR = 20\text{dB}$. (a) Same CM-1 signal and its estimation with ℓ_1 -norm minimization, estimation error of the channel coefficients vector for ℓ_1 -norm minimization = 0.0578; (b) Same CM-1 signal in (a) and its estimation with BCS, estimation error of the channel coefficients vector for BCS = 0.0120. | 27 |
| Figure 5.1 : Effect of the number of measurements on the MSE performances of BCS and ℓ_1 -norm minimization estimations for the channel models when $SNR = 20\text{dB}$ | 36 |
| Figure 5.2 : MSE performance comparison of BCS and ℓ_1 -norm minimization for CM-1. | 38 |
| Figure 5.3 : MSE performance comparison of BCS and ℓ_1 -norm minimization for CM-2. | 39 |
| Figure 5.4 : MSE performance comparison of BCS and ℓ_1 -norm minimization for CM-5. | 40 |

Figure 5.5 : MSE performance comparison of BCS and ℓ_1 -norm minimization for CM-8. 41

Figure A.1 : Principle of the Saleh-Valenzuela channel fading model [59]. 56

BAYESIAN COMPRESSIVE SENSING APPROACH FOR ULTRA-WIDEBAND CHANNEL ESTIMATION

SUMMARY

Ultra-Wideband (UWB) impulse radio (IR) is an emerging technology for wireless communications. Owing to distinguishing properties such as having low transmit power, low-cost simple structure, immunity to flat fading and capability of resolving multipath components individually with good time resolution, UWB-IRs have been selected as the physical layer structure of Wireless Personal Area Network (WPAN) standard IEEE 802.15.4a for location and ranging, and low data rate applications. In the implementation of UWB-IRs, one of the main challenges is the channel estimation. Due to ultra-wide bandwidth of UWB-IRs, the main disadvantage of implementing the conventional maximum likelihood (ML) channel estimator is that very high sampling rates, i.e., very high speed analog-to-digital (A/D) converters are required for precise channel estimation.

Reconstruction of sparse signals with a sampling rate significantly lower than Nyquist rate is possible with compressive sensing (CS). Due to the sparse structure of UWB channels, compressive sensing can be used for UWB channel estimation in order to overcome the high-rate sampling problem. Among various implementations of CS, the inclusion of Bayesian framework has shown potential to improve signal recovery as statistical information related to signal parameters is considered. Accordingly, the application of Bayesian CS (BCS) approach to the estimation of sparse UWB channels is considered in this study.

In this thesis, the channel estimation performance of BCS is studied for various UWB channel models and noise conditions. Specifically, the effects of (i) sparse structure of standardized IEEE 802.15.4a channel models, (ii) signal-to-noise ratio (SNR) regions, and (iii) number of measurements on the BCS channel estimation performance are investigated, and they are compared to the results of ℓ_1 -norm minimization based estimation, which is widely used for sparse channel estimation. Furthermore, a lower bound on mean-square error (MSE) is provided for the *biased* BCS estimator and it is compared with the MSE performance of implemented BCS estimator. Moreover, the computation efficiencies of BCS and ℓ_1 -norm minimization are investigated in terms of computation time by making use of the big- O notation.

The study shows that BCS exhibits superior performance at higher SNR regions for adequate number of measurements and sparser channel models (e.g., CM-1 and CM-2). Furthermore, BCS is found to be computationally more efficient compared to ℓ_1 -norm minimization. Based on the results of this thesis, the BCS method or the ℓ_1 -norm minimization method can be preferred over the other one for different system implementation conditions.

ULTRA GENİŞ BANT KANAL KESTİRİMİ İÇİN BAYES SIKIŞTIRILMIŞ ALGILAMA YAKLAŞIMI

ÖZET

Ultra geniş bant dürtü radyosu, kablosuz haberleşme için yeni gelişen bir teknolojidir. Amerika Birleşik Devletleri'nde haberleşme alanında düzenleyici kuruluş olan Federal Haberleşme Komisyonu (FCC) tarafından ultra geniş bant teknolojisiyle ilgili düzenlemeler yapıldıktan sonra öncelikle IEEE 802.15.3 standardı görev grubu, ultra geniş bant dürtü radyolarıyla yüksek hızlı kablosuz kişisel alan ağı uygulamaları için yeni bir fiziksel katman yapısı oluşturulması amacıyla 802.15.3a çalışma grubunu kurmuştur. Ultra geniş bant veri iletiminde iletim uzaklığındaki artış, veri hızında düşüşe neden olur. Bu doğrultuda IEEE 802.15.4 standardı görev grubu, ultra geniş bant dürtü radyolarıyla düşük hızlı fakat iletim uzaklığı daha büyük olan kablosuz kişisel alan ağı uygulamaları için yeni bir fiziksel katman yapısı oluşturulması amacıyla 802.15.4a çalışma grubunu kurmuştur. Bu çalışma grubu, özellikle ortalama bir veri hızı fakat düşük güç tüketimi, karmaşıklık ve maliyet gerektiren sensör ağı uygulamaları gibi uygulamalar üzerinde çalışmalarını yoğunlaştırmıştır. Bu çalışmada IEEE 802.15.4a bünyesindeki çeşitli ultra geniş bant kanal modellerinin kestirimi üzerine odaklanılmıştır.

Düşük iletim gücü, düşük maliyetli basit yapı, düz sönümlenmeye karşı bağımsızlık ve çokyollu bileşenleri iyi bir zaman çözünürlüğüyle ayrı ayrı çözme yeteneği gibi ayırt edici özelliklere sahip olması dolayısıyla ultra geniş bant dürtü radyoları, konumlama, uzaklık belirleme ve düşük veri hızlı uygulamalar için belirlenen kablosuz kişisel alan ağı IEEE 802.15.4a standardının fiziksel katman yapısı olarak seçilmiştir. Ultra geniş bant dürtü radyolarının gerçekleştiriminde karşılaşılan temel zorluklardan biri de kanal kestirimidir. Kanal karakteristikleri hakkında doğru bir bilgiye sahip olmak, haberleşme açısından etkin bir veri iletimi gerçekleştirmek ve sistem performansını artırmak için oldukça önemlidir. Bu nedenle kanal dürtü yanıtı hakkında bilgi edinmek için kanal kestirimi gereklidir. Ultra geniş bant dürtü radyolarının bantgenişliğinin çok fazla olması dolayısıyla, kanal kestiriminde klasik en büyük olabilirlik kestirimcisinin kullanılmasının başlıca dezavantajı, hassas bir kanal kestirimi için Nyquist kriterine göre alıcıdaki örnekleme işleminde çok yüksek örnekleme oranlarına, bir başka ifadeyle çok yüksek hızlı analog-sayısal dönüştürücülere ihtiyaç duyulmasıdır. Bu durum alıcıda devre karmaşıklığının ve maliyetin artmasına neden olur.

Yüksek örnekleme oranı gerektiren bu ultra geniş bant kanal kestirimi probleminin üstesinden gelmek için sıkıştırılmış algılama kullanılabilir. Sıkıştırılmış algılama yöntemi, Nyquist oranından önemli ölçüde daha düşük bir örnekleme oranıyla seyrek sinyallerin geri elde edilmesini mümkün kılmaktadır. Seyrek sinyal ifadesi en basit anlamda, bir çok bileşeni sıfır veya sıfıra yakın olan bir başka ifadeyle çok az bileşeni sıfırdan farklı olan sinyaller için kullanılan bir ifadedir. Alıcıda ard arda

alınan ultra geniş bant sinyaller kayda değer bir zaman gecikmesiyle alıcıya ulaştığı ve alıcıda ayrı ayrı çözülebildiği için ultra geniş bant çokyollu kanallar için seyrek yapıya sahip olma varsayımı yaygın kabul görmüştür. Ultra geniş bant kanalların bu özelliği nedeniyle sıkıştırılmış algılama yöntemi, yüksek örnekleme oranı probleminin üstesinden gelmek için ultra geniş bant kanal kestiriminde kullanılabilir. Böylece sıkıştırılmış algılama ile alıcının yüksek maliyeti, karmaşıklığı ve güç tüketimi azaltılarak daha basit yapıda bir alıcı, ultra geniş bant sistemde kullanılabilir.

Sıkıştırılmış algılama literatüründe, aynı zamanda basis pursuit (BP) olarak da bilinen ℓ_1 -norm enküçültme ve matching pursuit (MP) olmak üzere seyrek sinyal geri elde ediniminde kullanılan 2 temel algoritma vardır. Literatürde aynı zamanda bu algoritmaların basis pursuit de-noising (BPDN), orthogonal matching pursuit (OMP), stagewise orthogonal matching pursuit (StOMP) ve compressive sampling matching pursuit (CoSaMP) gibi çeşitli türevleri de bulunmaktadır. Son yıllarda Bayes yapının sıkıştırılmış algılama teorisine uygulanmasıyla birlikte, Bayes tabanlı çeşitli sıkıştırılmış algılama algoritmaları, sıkıştırılmış algılama literatürünün bir parçası olmaya başlamıştır. Bu tezde kullanılacak olan Bayes sıkıştırılmış algılama algoritması da bunlardan biridir. Sıkıştırılmış algılamanın bu çeşitli gerçekleştirmelerinin arasında Bayes yapının katkısı, ilgili sinyalin istatistiksel özellikleri de göz önünde bulundurulduğundan sinyal geri elde ediniminin iyileştirilmesi açısından önemli bir potansiyel göstermiştir. Bu doğrultuda, Bayes sıkıştırılmış algılama yaklaşımının seyrek ultra geniş bant kanalların kestirimine uygulanması bu çalışma ile gerçekleştirilmiştir.

Bu tezde gerçeğe uygun çeşitli ultra geniş bant kanal modelleri için Bayes sıkıştırılmış algılamanın kanal kestirim performansı incelenmiştir. Özellikle Bayes sıkıştırılmış algılama modelini doğrudan etkilediği için analiz açısından önemli olan (i) standartlaştırılmış IEEE 802.15.4a kanal modellerinin seyrek yapılarının, (ii) işaret-gürültü oranı seviyelerinin ve (iii) ölçüm sayısının çeşitli senaryolar için Bayes sıkıştırılmış algılama kanal kestirim performansı üzerindeki etkileri araştırılmış ve bu sonuçlar seyrek sinyal kestirimi için yaygın olarak kullanılan ℓ_1 -norm enküçültme tabanlı kestirim sonuçlarıyla karşılaştırılmıştır.

Sıkıştırılmış algılama tabanlı ultra geniş bant kanal kestiriminde önemli rol oynayan ultra geniş bant kanalların seyrek yapıya sahip olma varsayımı, kanal ortamları incelenerek doğrulanmalıdır. Bu nedenle tezde, çeşitli kanal ortamlarını modelleyerek oluşturulmuş ve ultra geniş bant araştırma çalışmalarında yaygın olarak kullanılan IEEE 802.15.4a standardı bünyesindeki kanal modeli-1, kanal modeli-2, kanal modeli-5 ve kanal modeli-8 olmak üzere 4 farklı kanal modeli göz önünde bulundurulmuştur. Kısaca bu kanal modellerinin belirgin karakteristikleri özetlenecek olursa:

Kanal modeli-1, alıcı verici arasında doğrudan görüşün (LOS) olduğu konut içi ortamı temsil eden ve IEEE 802.15.4a standardı bünyesindeki en seyrek yapıya sahip olan kanal modelidir.

Kanal modeli-2, alıcı verici arasında doğrudan görüşün olmadığı (NLOS) konut içi ortamı temsil eden kanal modelidir. Kanal modeli-2 de kanal modeli-1 gibi seyrek yapıya sahiptir fakat kanal modeli-1'e kıyasla daha fazla çokyollu bileşene sahiptir.

Kanal modeli-1 ve kanal modeli-2'nin temsil ettikleri ortam, kısa mesafedeki güvenlik ve ölçüm sensörlerinin bulunduğu ev ağları için oldukça önemlidir.

Kanal modeli-5, alıcı verici arasında doğrudan görüşün olduğu kapalı olmayan (açık alan) ortamı temsil eden kanal modelidir. Kanal modeli-1 ve kanal modeli-2'ye göre oldukça düşük seyrekliğe sahiptir. Bu kanal modelinde çokyollu bileşenler genellikle birkaç küme halindedir.

Kanal modeli-8, alıcı verici arasında doğrudan görüşün olmadığı endüstriyel ortamı temsil eden kanal modelidir. Ortam bir çok metal yansıtıcılarla dolu geniş fabrika holleri tarafından karakterize edilir. Böylesi bir ortam çok yoğun şekilde çokyollu bileşenlerin oluşmasına neden olur. Bu sebeple kanal modeli-8, seyrek kanal modeli olarak tanımlanamaz. Dolayısıyla bu 4 kanal modeli içinde en az seyrek yapıya sahip kanal modelidir.

Kestirim problemleri analizinde, olabilecek en iyi kestirimci hata performansını belirlemek, performans analizi için önemlidir. Performans alt sınırları da bu en iyi kestirimcinin hata performansını gösterdiği için gerçekleşen kestirimcinin hata performansının değerlendirilmesi açısından önemli bir değerlendirme ölçütüdür. Cramér-Rao alt sınırı yanlı olmayan (unbiased) kestirimciler için yaygın olarak kullanılan bir performans sınırıdır. Gerçekte Cramér-Rao alt sınırı, yanlı olmayan kestirimcilerin toplam varyansı üzerindeki bir alt sınırdır. Bununla birlikte yanlı olmayan kestirimciler için ortalama karesel hata varyansa eşit olduğu için, Cramér-Rao alt sınırı aynı zamanda kestirim hatası üzerindeki bir alt sınırdır. Ancak, bu çalışmada ultra geniş bant kanal kestirimi için önerilen Bayes sıkıştırılmış algılama kestirimcisi, Bayes bir kestirimci olmasının yanı sıra aynı zamanda yanlı (biased) bir kestirimcidir. Dolayısıyla kestirim hatası üzerinde değerlendirme ölçütü olarak bir performans alt sınırı belirlemek, Bayes sıkıştırılmış algılama kestirimcisinin performans analizi açısından önemlidir. Literatürde var olan sonsal (Posterior) Cramér-Rao alt sınırı veya Bayes Cramér-Rao alt sınırı, yanlı olmayan Bayes kestirimcilerin kestirim hatası değil de varyansları üzerindeki bir alt sınırdır. Cramér-Rao alt sınırına ek olarak sonsal Cramér-Rao alt sınırı için Bayes yapıdan dolayı kestirilecek parametre vektörüne ilişkin önsel (prior) olasılık dağılımı da göz önünde bulundurulur. Bu nedenle, bu çalışmada doğrusal yanlılık vektörlerine sahip yanlı Bayes kestirimciler için parametre vektörüne ilişkin önsel olasılık dağılımına ek olarak yanlılık terimi de göz önünde bulundurularak ortalama karesel hata üzerinde bir alt sınır sağlanmış ve bu ortalama karesel hata alt sınırı, gerçekleşen Bayes sıkıştırılmış algılama kestirimcisinin kanal kestirim performansıyla karşılaştırılmıştır. Dahası Bayes sıkıştırılmış algılama ve ℓ_1 -norm enküçültme yöntemlerinin işlemsel verimliliği büyük- O notasyonundan faydalanılarak işlem sürelerine göre incelenmiştir.

Çalışma sonucunda, Bayes sıkıştırılmış algılamanın yüksek işaret-gürültü oranı seviyelerinde yeterli sayıda ölçüm ve seyrek kanal modelleri (kanal modeli-1 ve kanal modeli-2) için ℓ_1 -norm enküçültme yöntemine kıyasla üstün bir performans sergilediği görülmüştür. Ayrıca ℓ_1 -norm enküçültme yöntemiyle karşılaştırıldığında, Bayes sıkıştırılmış algılama yönteminin işlemsel olarak daha verimli olduğu sonucu çıkarılmıştır. Bu tezin sonuçları göz önünde bulundurulduğunda, farklı sistem gerçekleştirim durumları için Bayes sıkıştırılmış algılama yöntemi veya ℓ_1 -norm enküçültme yöntemi diğerinin yerine tercih edilebilir.

1. INTRODUCTION

1.1 Motivation of the Thesis

In the last decade, there have been significant developments and advances in wireless communications which have become extensively a part of our lives nowadays. Moreover, demands on the wireless services have been increasing day by day with the technological advancements in communications. However, due to the limited structure of the electromagnetic spectrum, crowdedness of existing frequency bands with licensed systems and the growing demands on wireless services, newly developed systems have encountered important challenges such as frequency allocation in the spectrum. Therefore in recent years, efficient usage of the spectrum with spectrum sharing techniques have received great interest. To address this issue, ultra-wideband (UWB) impulse radio (IR) [1], an emerging technology in wireless communications, has received great interest from both academia and industry [2] owing to features such as low interference when sharing the spectrum with licensed systems due to its ultra-wide bandwidth and transmission with low power spectral density. This short-range wireless technology will play an important role in networks where everybody and everything in that short-range is connected each other with communication links. Low power consumption, low complexity and low cost transceiver structure, accurate ranging and positioning capabilities, high data rates, capability of resolving multipath components individually with fine time resolution due to its ultra-wide bandwidth, low probability of intercept and detection, immunity to interference, low susceptibility to multipath fading and superior material penetrating capability are remarkable features of the UWB technology.

Considering the distinguishing properties that are mentioned above, there are different applications of UWB in various fields such as through-wall [3] and in-wall detection, ground penetrating radar [4], medical imaging [5], construction and home repair

imaging, mining, surveillance systems [6] in radar imaging field; collision avoidance [7], roadside assistance [8] in vehicular radar imaging field; positioning, locating objects, monitoring infrastructure, perimeter intrusion detection in Wireless Sensor Networks (WSNs) [9], medical information gathering with body attached sensors in Wireless Body Area Networks (WBANs) [10] and high rate data communications with high wireless connectivity, location and ranging in Wireless Personal Area Networks (WPANs) in UWB communications field. In addition to these applications, the features that are mentioned above also make the use of UWB an attractive choice for future wireless applications.

Historically, the development of UWB is speeded up with the development of the sampling oscilloscope in the early 1960s and the corresponding techniques for generating sub-nanosecond baseband pulses [11]. Henning F. Harmuth at Catholic University of America and Gerald F. Ross and Kenneth W. Robins at Sperry Rand Corporation whose works accelerated the development of UWB, are some of the important pioneers of the modern UWB communications in the United States from the late 1960's. Gerald F. Ross became the owner of the first U.S. patent for UWB communications in 1973 [12]. Between the 1960's and the late 1990's, the development and applications of UWB were restricted to the military and works funded by the U.S. Department of Defense classified programs. Due to precise positioning capability and low probability of interception and detection, radar and high secure communication applications constitutes the military applications, where the term "ultra-wideband" was used by U.S. Department of Defense in 1989 for the first time. The commercial usage of UWB communication has started up in the late 1990s with the chipsets called PulsON and Trinity that developed by the Time Domain and XtremeSpectrum companies, respectively [11]. Thus, UWB technology has taken place in commercial applications as well as in military applications and it has been gaining more importance gradually.

UWB-IRs have been selected as the physical layer structure of WPAN standard IEEE 802.15.4a for location and ranging, and low data rate applications [13] owing to the remarkable properties that are specified above. In the implementation of UWB-IRs, one of the main challenges is the channel estimation. It is important to identify accurate

characteristics of the channel for the communication in order to realize an effective transmission and to improve the system performance. Accordingly, channel estimation is essential to acquire information about the channel impulse response. However, due to ultra-wide bandwidth of UWB-IRs, the main disadvantage of implementing the conventional maximum likelihood (ML) channel estimator [14, 15] is that very high sampling rates, i.e., very high speed analog-to-digital (A/D) converters are required for precise channel estimation and this causes the increasing of circuit complexity and cost at the receiver.

In order to overcome the high-rate sampling problem, compressive sensing (CS) theory proposed in [16–18] can be considered for UWB channel estimation. CS is a promising paradigm in signal processing, where a signal that is sparse in a known transform domain can be recovered with high probability from a set of random linear projections with much fewer measurements than usually required by the dimensions of this domain. As the received sequential UWB pulses arrive with a considerable time delay and can be resolved individually at the receiver, sparse structure assumption is widely accepted for UWB multipath channels. This property of UWB channels, makes the applicability of CS for the channel estimation possible.

There are state of the art algorithms such as ℓ_1 -norm minimization, also referred to as basis pursuit (BP), and matching pursuit (MP) which are used for the signal recovery in the CS literature. Also, variations of these algorithms such as basis pursuit de-noising (BPDN) (for the noisy case of BP), orthogonal matching pursuit (OMP), stagewise orthogonal matching pursuit (StOMP) and compressive sampling matching pursuit (CoSaMP) have been studied in the literature. In recent years, Bayes' theorem based CS algorithms have begun taking a part of CS literature with the application of Bayesian framework in CS theory, where Bayesian CS (BCS) is one of these algorithms. BCS exploits statistical information of the unknown signal for the estimation unlike the non-Bayes based algorithms that are mentioned above. Prior knowledge of the unknown signal is used in BCS. Hence in this thesis, the application of BCS to UWB channel estimation is realized and the improvement of UWB channel estimation performance is investigated by using BCS and compared to the ℓ_1 -norm minimization method, which is widely used method in CS based estimation.

Earlier works on UWB channel estimation and CS theory related to the content of this thesis are given in the next section.

1.2 Literature Review

Due to the high speed A/D converters requirement, reducing the complexity and cost of the receiver is the main concern in UWB-IR system design. Consequently, CS based UWB transceiver design and CS based UWB channel estimation topics have received great interest recently. In [19–22], CS based transceiver design is investigated, where the main purpose is the detection of the UWB signal with low sampling rate compared to Nyquist rate with the negligible performance deterioration and eventually reduction of the complexity and cost of the system. On the other hand, the CS theory which is proposed for sparse signal reconstruction can be applied for sparse channel estimation in communications [23, 24]. UWB multipath channels are qualified as having sparse structure since the received sequential UWB pulses arrive with a considerable time delay on account of having low duty-cycle. Accordingly, CS has been exploited for UWB channel estimation [25–28]. In [25], a channel detection and estimation method based on the MP algorithm is proposed. In [26], a pre-filtering method based on the OMP algorithm is proposed for UWB channel estimation. In [27], novel CS-based data detection and channel estimation approaches for UWB-IR systems are proposed by using MP and BPDN algorithms. In [28], the conventional ℓ_1 -norm minimization method has been used for the estimation of different UWB channel models.

Among various implementations of CS, one approach has been to include the Bayesian model. Considering the sparse Bayesian model in [29], a Bayesian framework has been developed for CS in [30]. In [31], a hierarchical form of Laplace priors on signal coefficients is taken into consideration for BCS. Both of the frameworks have shown potential to improve signal recovery as the posterior density function over the associated sparse channel coefficients is considered. In [32], a Turbo BCS algorithm for sparse signal reconstruction through exploiting and integrating spatial and temporal redundancies in multiple sparse signal reconstruction is proposed. In [33], the Laplace prior based BCS algorithm in [31] has been modified for joint reconstruction of received sparse signals and channel parameters for multiuser UWB communications.

In [34], the proposed approach in [30] is considered for UWB channel estimation, where BCS estimation results are compared to the ℓ_1 -norm minimization results. However, the effects of UWB channel models (i.e., sparsity condition) or additive noise level (i.e., Bayesian approach depends on the statistical information about channel parameters and additive noise) on the channel estimation performance have not been considered in [34]. These effects should be also quantified to generalize the CS based UWB channel estimation results.

1.3 Purpose of the Thesis

Motivated by investigating the factors that affect the performance of BCS in realistic UWB channels, the effects of (i) sparse structure of standardized IEEE 802.15.4a channel models, (ii) signal-to-noise ratio (SNR) regions, and (iii) number of measurements on the channel estimation performance are studied in this thesis. These factors are important to analyze as sparsity, noise level and measurements directly affect the BCS model. Accordingly, BCS channel estimation performance for various scenarios is compared to the ℓ_1 -norm minimization based estimation, which is a method widely used for sparse channel estimation. Furthermore, it is important to specify a lower bound on the estimation error as a benchmark for the performance analysis of BCS estimators. Posterior Cramér-Rao lower bound (PCRLB), also referred to as the Bayesian CRLB, is a widely used bound that defines a lower bound on the mean-square error (MSE) of *unbiased* Bayesian estimators [35]. Indeed, CRLB is a lower bound *only* on the total variance of *unbiased* estimators [36], where MSE becomes equal to the variance for *unbiased* estimators. However, for *biased* estimators the bias term should be taken into account in addition to the variance of the estimator. By considering the bound in [37], an MSE lower bound will be presented for *biased* Bayesian estimators with linear bias vectors to compare with the actual channel estimation performance of BCS. In addition, computation efficiency of BCS over the ℓ_1 -norm minimization will be justified in terms of computation time by making use of the big- O notation. The comparison results provided are important

in order to define the conditions where BCS may be preferred over the conventional ℓ_1 -norm minimization method.

1.4 Preview of the Thesis

In this first chapter, motivation of the thesis, literature review related to the subject of the thesis and the purpose of the thesis are presented. The rest of the thesis is organized as follows. In Chapter 2, basics of UWB communications are given in brief and IEEE 802.15.4a channel models that are widely used in UWB communications are explained. In Chapter 3, the overview of CS theory, ℓ_1 -norm minimization, Bayesian model and their applications to UWB channel estimation are presented. In Chapter 4, an MSE performance bound for a *biased* BCS estimator is provided. In Chapter 5, simulation results for performance comparison are presented and also computation efficiencies of both BCS and ℓ_1 -norm minimization are compared. Concluding remarks are given in Chapter 6.

2. ULTRA-WIDEBAND COMMUNICATIONS

2.1 Overview of Ultra-Wideband Communications

UWB is a promising technology and has a significant potential for short-range wireless communications due to its notable properties such as having high data rates, very good time resolution which allows precise positioning and ranging applications, immunity to multipath fading, low processing power and potential of allowing simple and low cost transceiver structure. Accordingly, these remarkable properties make UWB an attractive choice for applications of commercial communications [38]. Since interest in the commercialization of UWB systems has increased gradually from the late 1990s as mentioned in the Introduction chapter, frequency allocation for the UWB systems in the spectrum becomes an important issue due to their ultra-wide bandwidth range. Especially, developers of UWB systems began pressuring the Federal Communications Commission (FCC) that is the regulatory body in U.S., to approve regulatory review of UWB for commercial usage. Consequently, the FCC report [39] which included the authorization of different commercial unlicensed uses of UWB in the frequency range of 3.1 – 10.6 GHz for communications appeared in April 2002. According to the FCC rulings, a transmission which is realized with signals that has bandwidth (BW) greater than 500 MHz or fractional bandwidth (B_f) equal or greater than 0.2 is defined as an UWB transmission.

$$BW > 500 \text{ MHz} \quad \text{or} \quad B_f \geq 0.2 \quad (2.1)$$

The fractional bandwidth is expressed as the ratio of signal bandwidth to center frequency (f_c) [39]

$$B_f = \frac{BW}{f_c} = \frac{(f_H - f_L)}{(f_H + f_L)/2}, \quad (2.2)$$

where f_H and f_L are the upper and lower frequencies, respectively, at -10dB below the peak emission point. For the various regions of the spectrum, different allowed power spectral densities should be determined in order to avoid interference with existing

communication systems. Hence, the FCC has assigned allowed effective isotropic radiated power (EIRP), which is the power radiated by an omnidirectional antenna with gain 1, limit for frequency bands of UWB [40]. Accordingly, for the UWB communication systems, FCC radiation limit is determined as -41.3 dBm/MHz (75 nW/MHz) in the frequency range of $3.1 - 10.6$ GHz [39]. This is the limit (FCC Part 15 limit) of interference to the existing communication systems and also the limit of protection from the existing radio services. For this purpose, FCC has assigned two spectral masks for the indoor and outdoor UWB communication systems which are given in Figures 2.1 and 2.2, respectively.

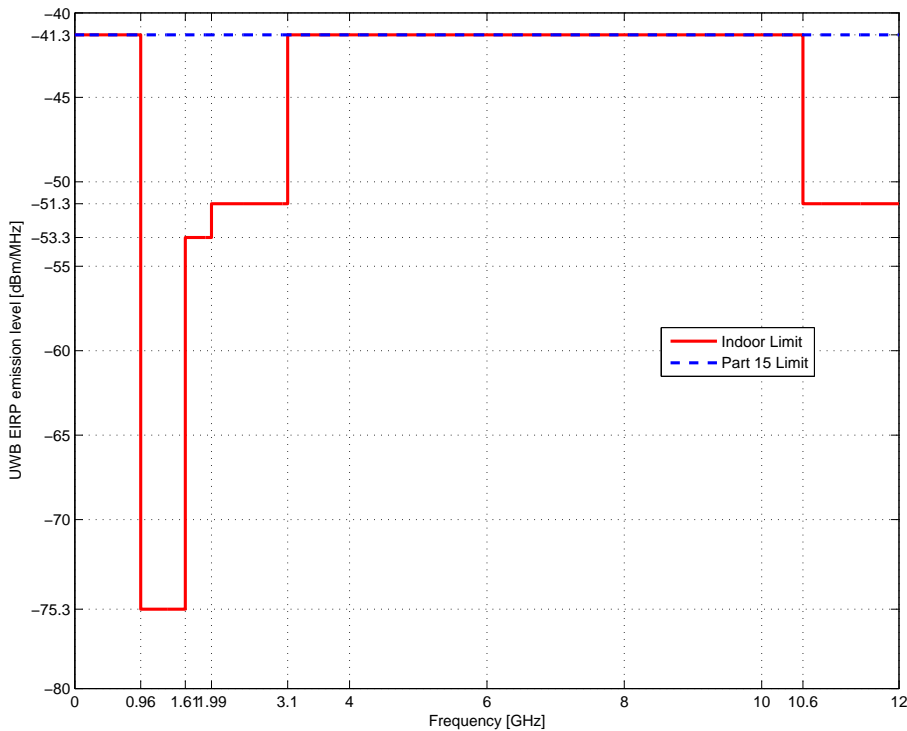


Figure 2.1 : FCC spectral mask for indoor UWB communication systems.

While the radiation limits in the $3.1 - 10.6$ GHz frequency range are the same for both indoor and outdoor masks, the only difference is in the $1.61 - 3.1$ GHz frequency range where the indoor radiation limit is 10 dB greater than the outdoor radiation limit. For particular susceptible frequency bands such as the global positioning system (GPS) band ($0.96 - 1.16$ GHz), although the radiation limit is the same for both indoor and outdoor UWB systems, it is much lower compared to Part 15 limit in order to minimize

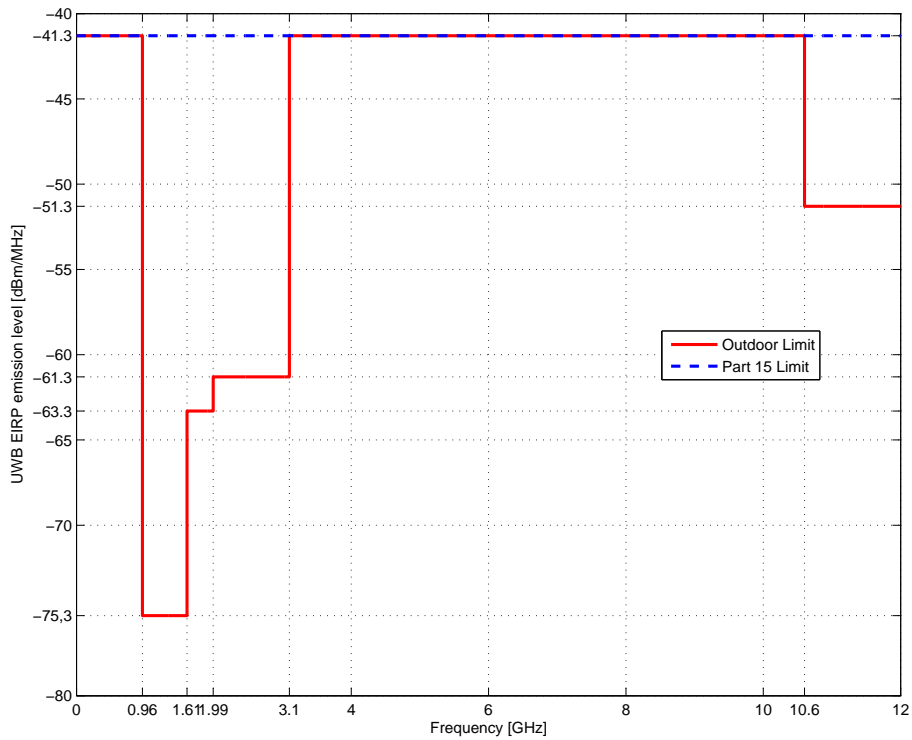


Figure 2.2 : FCC spectral mask for outdoor UWB communication systems.

the interference with GPS. A comparison of spectrum allocations of UWB and existing narrowband wireless communication systems with respect to emitted signal power is given in Figure 2.3. It is seen from the figure that the signal power of UWB systems is significantly lower than the other narrowband systems.

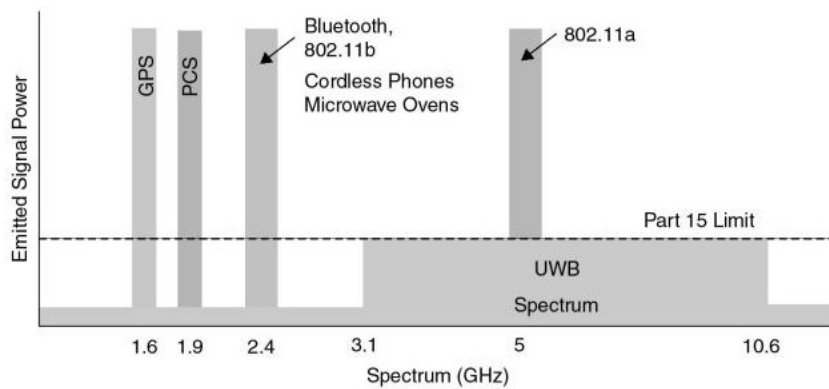


Figure 2.3 : Spectrum of UWB and existing narrowband communication systems [41].

After the FCC regulations, standardization works on the UWB technology has speeded up. UWB technology offers significant potential for wireless communication systems: (i) high data rate short-range communications (high data rate WPANs), (ii) low

data rate mid-range communications (low data rate WPANs, positioning and sensor networks). 802.15.3 standard task group of IEEE, has established the 802.15.3a study group (TG3a) in order to characterize a new physical layer notion for high data rate WPAN applications. In the UWB transmission, an increase in transmission range is provided with trading a reduction in data rate. Accordingly, IEEE 802.15.4 standard task group has also established the 802.15.4a study group (TG4a) to characterize a new physical layer notion for low data rate WPAN applications. The study group addressed applications which require moderate data rate but low power consumption and low complexity and cost, such as sensor network applications [41]. This study is focused on the estimation of UWB channels which are involved in IEEE 802.15.4a standard.

In the UWB communications, ultra-short pulses, whose time durations on the order of nanoseconds, with relatively low energy are used for the transmission of information. IR refers to the generation of a sequence of these ultra-short (impulse-like) waveforms (also referred to as monocycles). Since these ultra-short pulses are used, UWB signals have low sensitivity to multipath fading, which occurs when a modulated signal arrives at a receiver from different paths. Thus, these dense reflected paths can be resolved with fine time resolution at the receiver and it provides rich multipath diversity. The data which will be transmitted, is modulated directly into the sequence of ultra-short pulses. Data can be modulated using modulation techniques such as binary phase shift keying (BPSK) also known as bi-phase modulation or pulse position modulation (PPM) which are widely used in UWB communications. This type of signal transmission does not require a carrier since the pulse can propagate well in the radio channel. Therefore, such a transmission enables the low complexity and low cost of UWB systems with low power consumption by eliminating up/down-conversion processes and radio frequency (RF) mixing stage which are required in conventional radio technology [41].

Monocycle can be any pulse shape whose spectrum satisfies the FCC spectral requirements for UWB signals. The Gaussian pulses and its higher order derivatives are frequently used in the UWB systems as they can be easily generated by pulse generators (in comparison with the rectangular pulses that have very short rise and fall time). A typical widely used UWB pulse shape, which is the second derivative of a

Gaussian monocycle given in Figure 2.4, can be expressed as [1]

$$p(t) = A \left(1 - 4\pi \left[\frac{t - \mu}{d_w} \right]^2 \right) \exp \left(-2\pi \left[\frac{t - \mu}{d_w} \right]^2 \right), \quad (2.3)$$

where A is the amplitude of the pulse, μ denotes the location of the pulse center and d_w is the parameter that determines the pulse width.

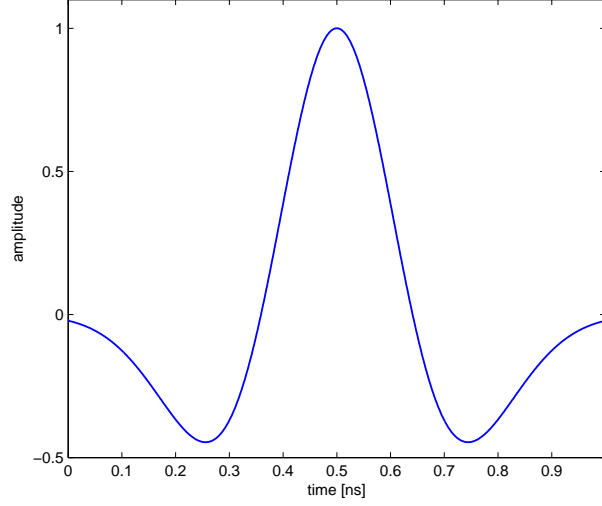


Figure 2.4 : A typical UWB pulse shape.

In BPSK modulation, the binary data is encoded in the polarity of the pulses. A BPSK modulated signal shown in Figure 2.5, can be expressed as

$$s(t) = \sum_{i=-\infty}^{\infty} a_i p(t - kT_f), \quad (2.4)$$

where $a_i \in \{+1, -1\}$ denotes the polarity of the modulated pulse and T_f is the frame duration and also known as pulse repetition interval. If the information bit is 1, a_i becomes +1; otherwise if the information bit is 0, a_i becomes -1 .



Figure 2.5 : An UWB BPSK modulated signal.

However, the most preferable modulation technique is PPM in the UWB literature [41]. In the UWB-IR transmission, the pulses are sent at regular time intervals from the transmitter and due to this pulse repetition in time, peaks called "spectral lines" or

"comb lines" appear in the power spectral density of transmitted UWB signal at the locations which are multiples of the inverse of pulse repetition interval [42]. Since these peaks exceeds the FCC Part 15 limit easily and causes interference with the other operating communication systems, they are undesirable. PPM minimizes these spectral peaks by encoding the data in the fine time shift of the pulses. Since the information is carried with the positions of pulses in PPM, it is less sensitive to noise than BPSK. An M -ary PPM modulated signal shown in Figure 2.6, can be expressed as

$$s(t) = \sum_{i=-\infty}^{\infty} p(t - iT_f - m_i T_d), \quad (2.5)$$

where $m_i \in \{0, 1, \dots, M - 1\}$ is the i th M -ary symbol and T_d denotes the modulation time shift.

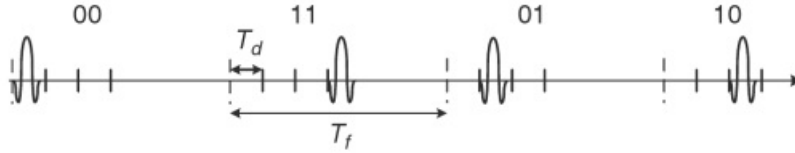


Figure 2.6 : An UWB 4-ary PPM modulated signal.

In Figure 2.7, a transmitted PPM modulated UWB signal, which has low duty cycle pulses, is given when $T_f = 20$ ns. Due to the low duty cycle nature of pulses, it is seen from the figure that the transmitted signal has a sparse structure.

This UWB signal, which is sent from the transmitter, reaches to the receiver after passing through the UWB channel. The signal is corrupted with destructive effects such as fading and noise in the channel. Mathematically, the transmitted modulated signal is convolved with channel impulse response (CIR) and noise is added to the signal, when it arrives the receiver antenna. This received signal can be expressed as

$$r(t) = \int_{-\infty}^{\infty} s(l)h(t-l)dl + n(t), \quad (2.6)$$

where $r(t)$, $s(t)$, $h(t)$, $n(t)$ denotes the received signal, the transmitted modulated signal, CIR of the UWB channel and the additive noise, respectively. BPSK or PPM modulated data can be detected coherent receiver structures, where Rake receivers are used [41, 42]. Accordingly, in order to determine the transmitted signal accurately at the receiver, a knowledge about the UWB channel characteristics is required. In other

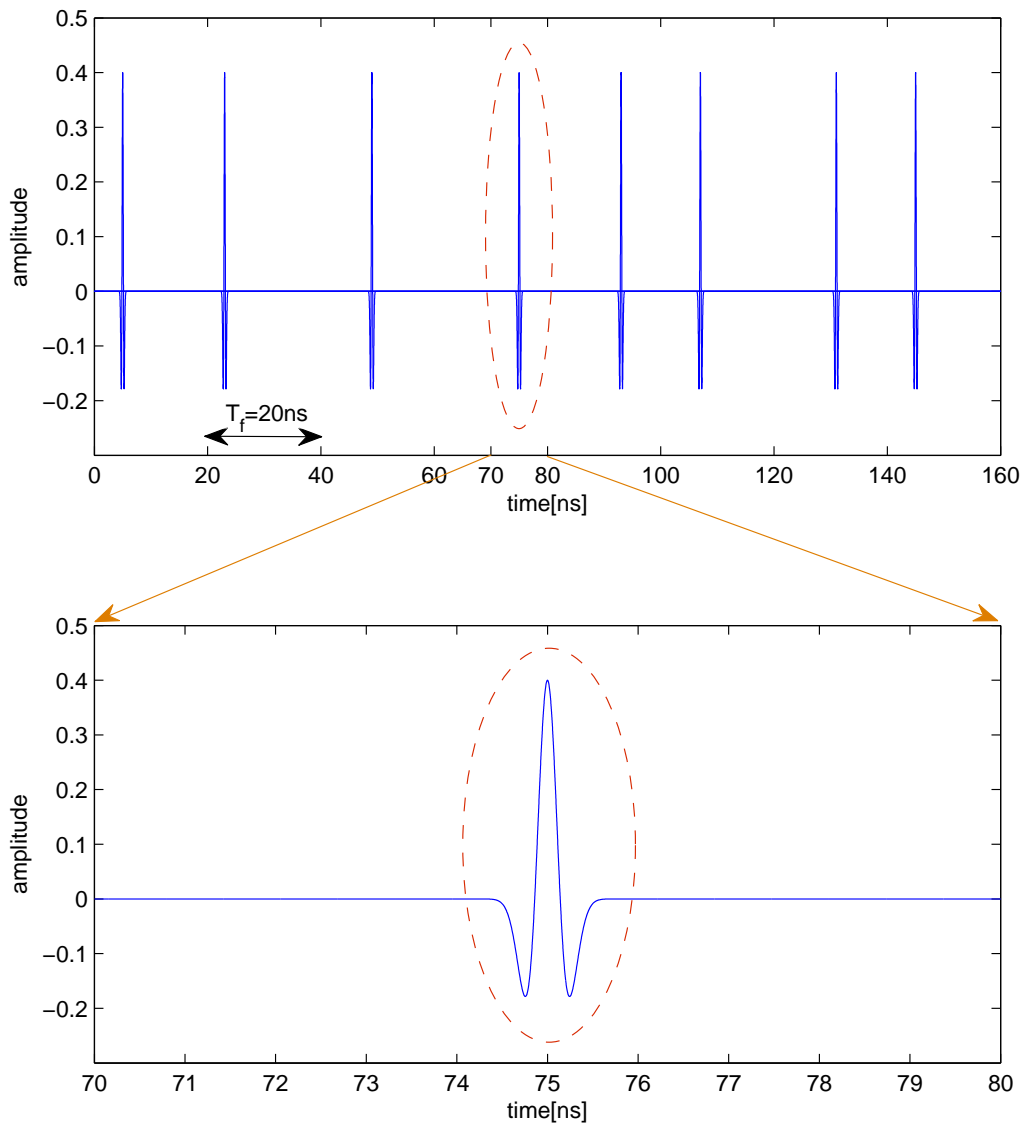


Figure 2.7 : A transmitted PPM modulated UWB signal.

words, it is necessary to know the channel impulse response of the UWB channel, which shows the channel characteristics of the UWB channel, to obtain the transmitted signal accurately from the received signal considering the channel effects. Therefore, in the next section, CIR of the UWB channels according to the channel models and channel models that we used in this thesis will be presented, respectively.

2.2 Ultra-Wideband Channel Model

In this section, the discrete-time equivalent UWB channel model and the standardized IEEE 802.15.4a channel models are presented, respectively.

In order to obtain the discrete-time channel model, the general CIR should be presented first. Accordingly, the continuous-time channel $h(t)$ can be modeled as

$$h(t) = \sum_{k=1}^{L_r} h_k \delta(t - \tau_k), \quad (2.7)$$

where h_k represents the k th multipath gain coefficient, τ_k is the delay of the k th multipath component, $\delta(\cdot)$ is the Dirac delta function and L_r represents the number of resolvable multipaths.

The continuous-time CIR given in (2.7) assumes that multipaths may arrive any time. This is referred to as the τ -spaced channel model [43]. Suppose that two sequential multipaths with delays τ_m and τ_{m+1} arrive very close to each other. Further suppose that a pulse with T_s -duration is transmitted through this channel. If $T_s > |\tau_m - \tau_{m+1}|$, then the pulse at the receiver cannot be resolved individually for each path, and it is concluded the combined channel response of the m th and $(m+1)$ th paths. Let us define an approximate T_s -spaced channel model that combines multipaths arriving in the same time bin, $[(n-1)T_s, nT_s], \forall n$. Accordingly, for $[(n-1)T_s, nT_s], \forall n$, the delays $\{\tau_k | 1, 2, \dots, L_r\}$ that arrive in the corresponding quantized time bins can be determined, and the associated $\{h_k | 1, 2, \dots, L_r\}$ gains can be linearly combined to give the new channel coefficients $\{c_n | 1, 2, \dots, N\}$. Note that some of the c_n values may be zero due to no arrival during that time bin. The equivalent T_s -spaced channel model can be expressed as

$$h(t) = \sum_{n=1}^N c_n \delta(t - nT_s), \quad (2.8)$$

where $T_c = NT_s$ is the channel length. Using (2.8), the discrete-time equivalent channel can be written as

$$\mathbf{h} = [c_1, c_2, \dots, c_N]^T, \quad (2.9)$$

where the channel resolution is T_s . Assuming that \mathbf{h} has K nonzero coefficients, the sparsity assumption of (2.9) is valid if $K \ll N$.

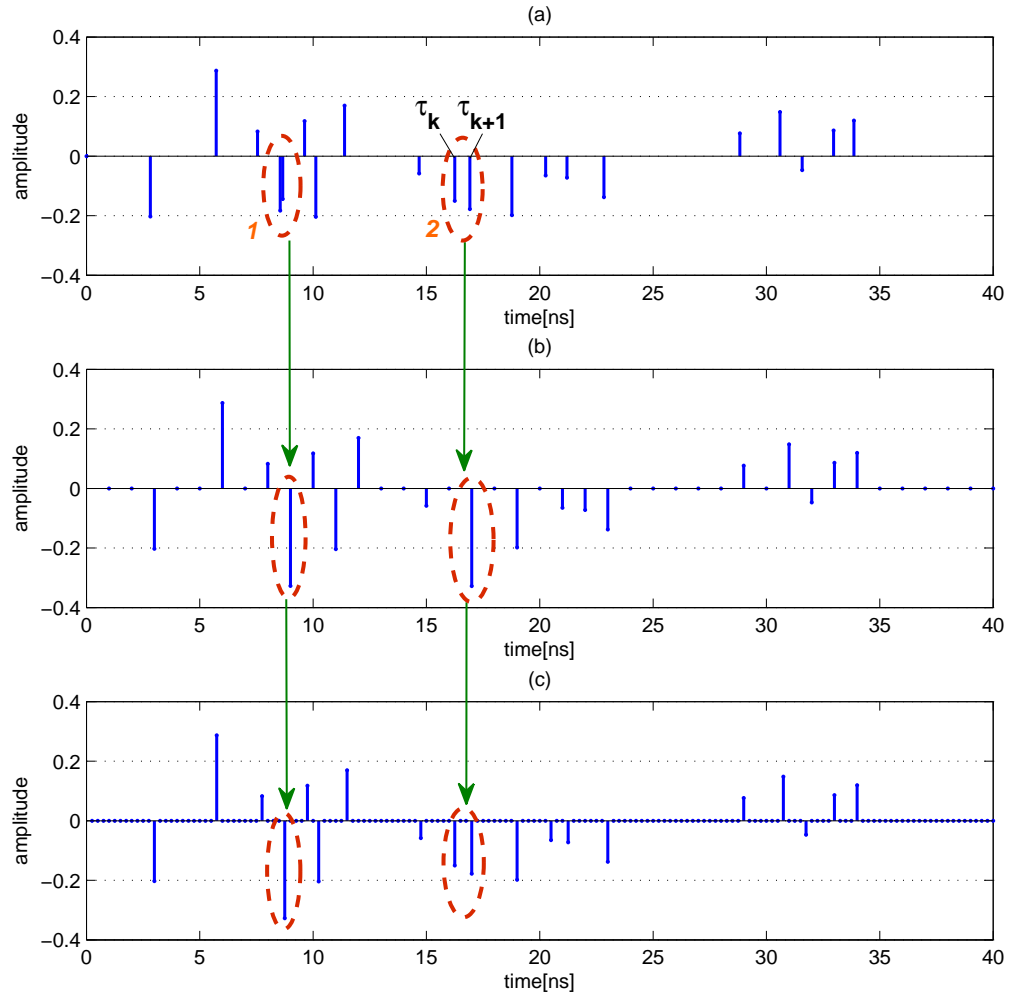


Figure 2.8 : The equivalent T_s -spaced channel model example. (a) UWB continuous time CIR; (b) T_s -spaced CIR when $T_s = 1\text{ns}$; (c) T_s -spaced CIR when $T_s = 0.25\text{ns}$.

An example for the equivalent T_s -spaced channel model explained above is given in Figure 2.8. In the first dashed circle (which is indicated with number 1) in Figure 2.8(a), absolute value of the difference between the delays of two consecutive multipaths is equal to $|\tau_k - \tau_{k+1}| = 0.1089\text{ns}$. Since the considered T_s values (1ns, 0.25ns) in Figure 2.8(b) and (c) are greater than this value, the sum of these two multipaths is acquired to give the new channel coefficient in Figure 2.8(b) and (c). On the other hand, absolute value of the difference between the delays of two consecutive multipaths is equal to $|\tau_k - \tau_{k+1}| = 0.6676\text{ns}$ in the second dashed circle (which is indicated with number 2) in Figure 2.8(a). Since the value of $T_s = 1\text{ns}$ is greater than this absolute value, the sum of these two multipaths is acquired to give the new

channel coefficient in Figure 2.8(b) as the consecutive multipaths cannot be resolved individually at the receiver. However in Figure 2.8(c), the value of $T_s = 0.25\text{ns}$ is smaller than this absolute value, and therefore, the two consecutive multipaths in the second dashed circle are represented individually.

Based on the discrete-time equivalent channel model above, the UWB channels are widely accepted as having a sparse structure. This assumption for UWB channels plays an important role in CS based UWB channel estimation. However, the channel environment should be inspected to prove this assumption. In [44], a comprehensive model for UWB propagation channels, which was accepted as the standardized channel model for IEEE 802.15.4a, has been developed considering various channel environments and conducting different measurement campaigns. These environments include indoor residential, indoor office, outdoor, industrial environments, agricultural areas and body area networks with having either a line-of-sight (LOS) or a non-LOS (NLOS) transmitter-receiver connection. In [28], the sparsity assumption of UWB channels has been discussed over the widely used channel models CM-1, CM-2, CM-5 and CM-8. In order to investigate the effects of channel sparsity on the BCS channel estimation performance, the same channel models are considered also in this study. Salient characteristics of these channel models can be expressed briefly as follows:

CM-1 is a channel model with a LOS connection in a residential indoor environment. It has the most sparse structure among the channel models for IEEE 802.15.4a and also it is frequently used channel model to qualify performance of the UWB systems.

CM-2 models a NLOS connection in a residential indoor environment where is the same as in CM-1. It has also sparse structure but there are more multipath components in CM-2 compared to CM-1. The environment of CM-1 and CM-2 (indoor residential) is crucial for home networking, connecting different devices as well as safety and measurement sensors in a short-range.

CM-5 is a channel model with a LOS connection in an outdoor environment. Although there are various outdoor scenarios, this model covers only a suburban-like microcell scenario, with a relatively short-range. It has a significantly less sparse structure compared to CM-1 and CM-2. Typically, multipaths arrive in a few clusters.

CM-8 models a NLOS connection in an industrial environment. The environment is

characterized by larger factory halls which are filled with a lot of metallic reflectors. This causes the issue of arriving the multipaths so densely and hence, CM-8 is not qualified as a sparse channel model. It has the least sparse structure among the channel models considered.

Single channel realizations of CM-1, CM-2, CM-5 and CM-8 with the parameters given in Appendix A are plotted in Figure 2.9 for illustrative purposes. For the implementations, the channel length and resolution are fixed to $T_c = 250\text{ns}$ and $T_s = 0.25\text{ns}$, respectively, resulting in the discrete-time channel length $N = T_c/T_s = 1000$.

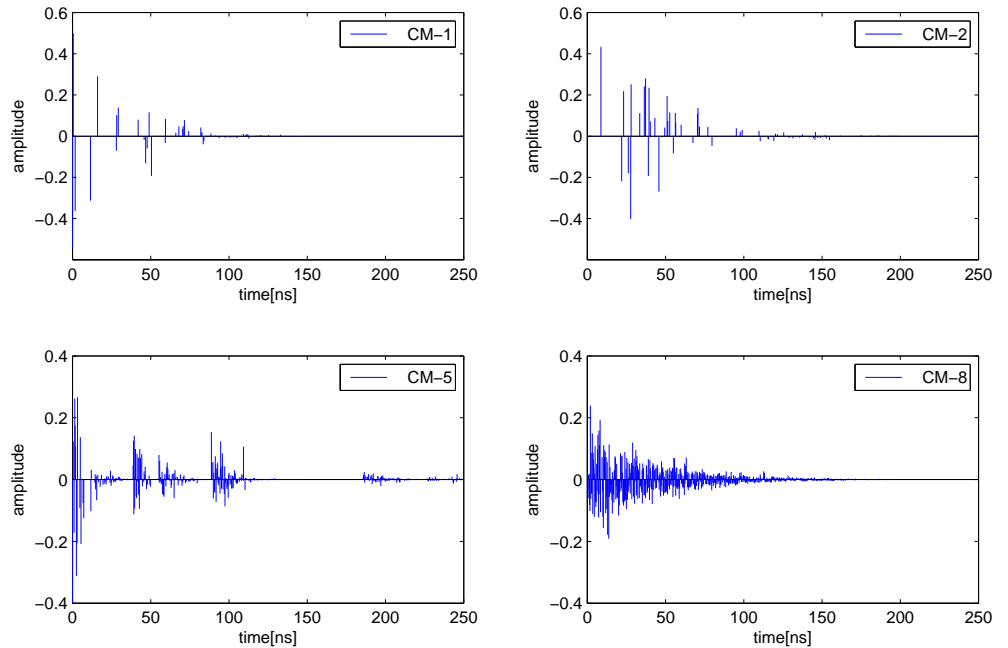


Figure 2.9 : Realizations of channel models when $T_c = 250\text{ns}$ and $T_s = 0.25\text{ns}$.

Here, K/N can be regarded as the sparsity ratio (i.e., the ratio of number of nonzero coefficients to the length of the equivalent discrete-time channel). The channel models' sparsity ratios, which are acquired by averaging over 200 channel realizations, for fixed $T_c = 250$ and $T_s = 0.25\text{ns}$ values are given in Table 2.1. It is crucial to determine accurate channel length (T_c) for the implementation in order to take account of all multipaths with considering delay of the multipaths. Although the value of $T_c = 100\text{ns}$ is adequate for CM-1 and CM-2, considering the CM-5 and CM-8 which include dense multipaths, for a fair comparison, channel length is determined as $T_c = 250\text{ns}$ for all channel models. Besides, the value of channel resolution (T_s) is also important to

resolve the multipaths at the receiver. Small value of channel resolution helps resolving the multipaths individually possible. Therefore, channel resolution is determined as $T_s = 0.25\text{ns}$. Furthermore, a smaller choice of T_s value makes the channel sparser [28].

Table 2.1 : Sparsity ratios of channel models when $T_c = 250\text{ns}$ and $T_s = 0.25\text{ns}$.

| Channel model | Sparsity ratio (K/N) |
|---------------|--------------------------|
| CM-1 | 0.06 |
| CM-2 | 0.09 |
| CM-5 | 0.47 |
| CM-8 | 0.79 |

3. COMPRESSIVE SENSING FOR UWB CHANNEL ESTIMATION

Due to the ultra-wide bandwidth of UWB-IRs, very high speed and complex A/D converters are required for sampling process at the receiver according to the conventional Nyquist criteria (the sampling rate must be at least twice the maximum frequency of the signal). However, it is known that the UWB channel has a sparse structure (see Section 2.2). Due to this sparsity prior knowledge about the channel, the emerging framework CS can be employed for UWB channel estimation in order to overcome the high-rate sampling problem. CS theory asserts that recovering sparse signals from fewer measurements corresponds to lower sampling rate than required for conventional methods [45]. Thus, more simple receiver structure can be used in the UWB system by reducing high cost, complexity and power consumption of the receiver with the CS. In the following, the overview of CS theory, ℓ_1 -norm minimization and its application to UWB channel estimation, and the Bayesian CS model will be presented, respectively.

3.1 Overview of Compressive Sensing

Consider the problem of reconstructing a discrete-time signal $\mathbf{x} \in \mathfrak{R}^N$ which can be represented in an arbitrary basis $\Psi \in \mathfrak{R}^{N \times N}$ with the weighting coefficients $\boldsymbol{\theta} \in \mathfrak{R}^N$ as

$$\mathbf{x} = \sum_{n=1}^N \psi_n \theta_n = \Psi \boldsymbol{\theta}. \quad (3.1)$$

Suppose that $\boldsymbol{\theta} = [\theta_1, \theta_2, \dots, \theta_N]^T$ has only K nonzero coefficients, where $K \ll N$ and $\Psi = [\psi_1, \psi_2, \dots, \psi_N]$. As \mathbf{x} is a linear combination of only K basis vectors, it can be called a K -sparse signal and can be expressed as

$$\mathbf{x} = \sum_{i=1}^K \psi_{n_i} \theta_{n_i}, \quad (3.2)$$

where $\{n_i\}$'s are the indices that correspond to nonzero coefficients. By projecting \mathbf{x} onto a random measurement matrix $\Phi \in \mathfrak{R}^{M \times N}$, a set of measurements $\mathbf{y} \in \mathfrak{R}^M$ can be

obtained as

$$\mathbf{y} = \Phi\Psi\boldsymbol{\theta}, \quad (3.3)$$

and it is shown in Figure 3.1 where $M \ll N$.

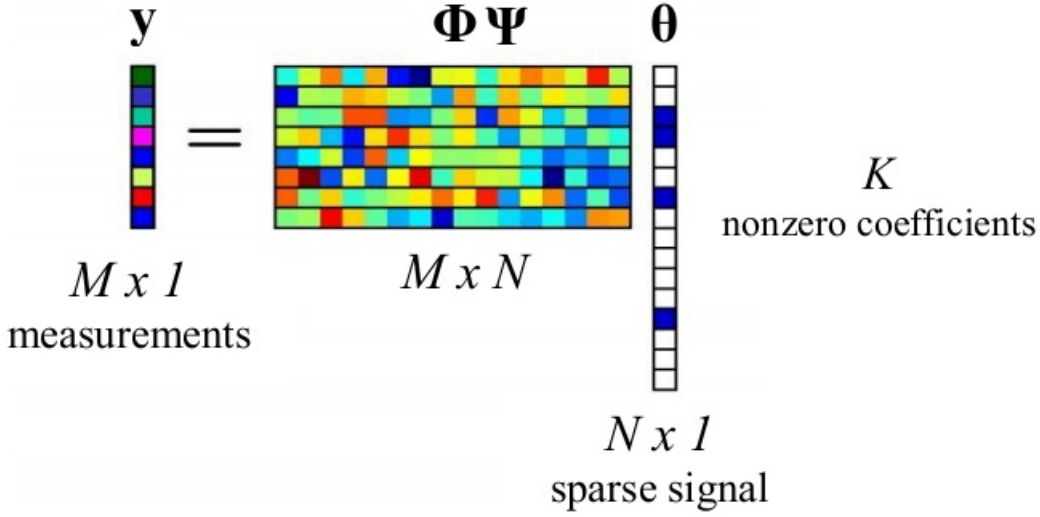


Figure 3.1 : Model of the compressive sensing.

In (3.3), the measurements \mathbf{y} , the measurement matrix Φ and the basis Ψ where the signal is sparse are known and $\boldsymbol{\theta}$ thereby \mathbf{x} are wanted to estimate. However due to $M \ll N$, the problem of solving $\boldsymbol{\theta}$ from (3.3) is underdetermined¹ and there are infinitely many solutions for $\boldsymbol{\theta}$ in (3.3). In order to choose an accurate solution to such an underdetermined system, additional appropriate constraints should be imposed. The solution to this underdetermined system of equations can be found via the CS by using the constraint of sparsity. CS seeks the sparsest solution (which have smallest number of nonzero coefficients) of $\boldsymbol{\theta}$ that satisfies the system of equations in (3.3). Accordingly, $\boldsymbol{\theta}$ can be estimated as

$$\hat{\boldsymbol{\theta}} = \min \|\boldsymbol{\theta}\|_0 \quad \text{subject to } \mathbf{y} = \Phi\Psi\boldsymbol{\theta}, \quad (3.4)$$

where $\|\cdot\|_0$ denotes ℓ_0 -norm, which is the number of nonzeros in its argument. Unfortunately, this combinatorial minimization problem is computationally intractable due to the search space of solutions being exponentially large [17, 46]. Therefore, ℓ_2 -norm minimization (least squares solution) can be proposed instead of ℓ_0 -norm

¹An underdetermined linear system has fewer equations than unknowns and generally has an infinite number of solutions.

minimization for the solution of $\boldsymbol{\theta}$ in (3.3) where ℓ_p -norm is denoted as $\|\boldsymbol{\theta}\|_p = (\sum_{n=1}^N |\theta_n|^p)^{\frac{1}{p}}$ for a real number $1 \leq p < \infty$. However, this method does not promote sparsity for the solution, spreads the energy of signal to all coefficients and leads to a poor result. On the other hand, ℓ_1 -norm minimization tends to concentrate energy of the signal on to nonzero coefficients and promotes sparsity. Hence, it provides a good approximation to ℓ_0 -norm minimization and it is tractable compared to ℓ_0 -norm minimization [47]. If $\boldsymbol{\theta}$ becomes sufficiently sparse, then the solution found with ℓ_1 -norm minimization will be quite close to the solution of ℓ_0 -norm minimization [48]. Accordingly, instead of ℓ_0 -norm minimization, $\boldsymbol{\theta}$ can be estimated as

$$\hat{\boldsymbol{\theta}} = \min \|\boldsymbol{\theta}\|_1 \quad \text{subject to } \mathbf{y} = \boldsymbol{\Phi}\boldsymbol{\Psi}\boldsymbol{\theta}. \quad (3.5)$$

The reconstruction problem hence becomes an ℓ_1 -norm optimization problem, and estimating $\boldsymbol{\theta}$ from the vector \mathbf{y} instead of \mathbf{x} corresponds to a lower sampling rate at the receiver. In (3.3), the measurement matrix should be incoherent with the basis in addition to the sparsity condition for accurately estimating the weighting coefficients. The incoherency is usually achieved by random matrices with independent identically distributed (i.i.d) elements from Gaussian or Bernoulli distributions [45]. Instead of using the N -sample \mathbf{x} to estimate the weighting coefficients $\boldsymbol{\theta}$, the M -sample measurement vector \mathbf{y} can be used.

The CS theory explained in (3.1)-(3.3) and (3.5) can be employed to UWB channel estimation. Suppose that $\mathbf{g} \in \mathfrak{R}^N$ is the discrete-time representation of the received signal given as

$$\mathbf{g} = \mathbf{P}\mathbf{h} + \mathbf{n}, \quad (3.6)$$

where $\mathbf{P} \in \mathfrak{R}^{N \times N}$ is a scalar matrix representing the time-shifted pulses, $\mathbf{h} = [c_1, c_2, \dots, c_N]^T$ are the channel gain coefficients, and \mathbf{n} are the additive white Gaussian noise (AWGN) terms. Since the UWB channel structure is sparse, \mathbf{h} has only K nonzero coefficients. Similar to (3.3), the received signal \mathbf{g} can be projected onto a random measurement matrix $\boldsymbol{\Phi} \in \mathfrak{R}^{M \times N}$ so as to obtain $\mathbf{y} \in \mathfrak{R}^M$ as

$$\begin{aligned} \mathbf{y} &= \boldsymbol{\Phi}\mathbf{P}\mathbf{h} + \boldsymbol{\Phi}\mathbf{n} \\ &= \mathbf{A}\mathbf{h} + \mathbf{z}. \end{aligned} \quad (3.7)$$

Due to the presence of the noise term \mathbf{z} , the channel \mathbf{h} can be estimated as

$$\hat{\mathbf{h}} = \min \|\mathbf{h}\|_1 \quad \text{subject to} \quad \|\mathbf{y} - \mathbf{A}\mathbf{h}\|_2 \leq \varepsilon, \quad (3.8)$$

where ε is related to the noise term as $\varepsilon \geq \|\mathbf{z}\|_2$. The ℓ_1 -norm minimization problem in (3.8) can be recast as a second-order cone program (SOCP) and solved² with a generic log-barrier algorithm.

3.2 Bayesian Compressive Sensing

In this section, the CS problem will be presented from a Bayesian perspective for UWB channel estimation. However, before presenting BCS theory, a short discussion about Bayes' theorem is provided.

The main aspect of Bayesian statistical approach is to define a probability about degree of belief on the unknown parameter based on the noisy observation data and prior information about the unknown parameter. Let us consider the problem of making inference about an unknown parameter vector \mathbf{t} from a noisy observation data vector \mathbf{r} . For the uncertainty about parameter vector, a prior distribution is defined (which expresses a known belief) on the unknown parameter vector \mathbf{t} before data are observed. By accounting observation data, a statistical model called likelihood is chosen to describe all the information about the acquired data that related to the underlying unknown parameter vector. Combining all these together gives Bayes' theorem as

$$p(\mathbf{t}|\mathbf{r}) = \frac{p(\mathbf{r}|\mathbf{t})p(\mathbf{t})}{p(\mathbf{r})}, \quad (3.9)$$

where $p(\mathbf{t}|\mathbf{r})$ is the posterior distribution over the unknown parameter vector \mathbf{t} , $p(\mathbf{t})$ is the prior distribution that describes the knowledge about \mathbf{t} , $p(\mathbf{r}|\mathbf{t})$ is the likelihood function which includes all information about the observation data \mathbf{r} and $p(\mathbf{r})$ is the marginal distribution of the \mathbf{r} which can be also expressed as $p(\mathbf{r}) = \int p(\mathbf{r}|\mathbf{t})p(\mathbf{t})d\mathbf{t}$. Mainly with the Bayes' theorem, the prior statistical information about the unknown parameter is updated to the posterior statistical information by using the observation data.

²For the implementation of (3.8), the codes provided by Romberg and Candès publicly available at <http://users.ece.gatech.edu/~justin/l1magic/> are used.

In the BCS framework proposed in [29, 30], the statistical information about the compressible signal and the additive noise is considered, where ℓ_1 -norm minimization does not consider these factors. Considering sparsity prior of \mathbf{h} and the noise model assumption together with the signal model in (3.7), BCS can be used³ for UWB channel estimation. Taking into consideration (3.7), the full posterior distribution over all unknowns of interest for the problem at hand becomes

$$p(\mathbf{h}, \boldsymbol{\beta}, \sigma^2 | \mathbf{y}) = \frac{p(\mathbf{y} | \mathbf{h}, \boldsymbol{\beta}, \sigma^2) p(\mathbf{h}, \boldsymbol{\beta}, \sigma^2)}{p(\mathbf{y})}, \quad (3.10)$$

where $\boldsymbol{\beta}$ represents hyperparameters that control the inverse variance of each channel coefficient, and σ^2 is the variance of each noise term in \mathbf{z} . Unfortunately, this full posterior term is not tractable since the integral

$$p(\mathbf{y}) = \int \int \int p(\mathbf{y} | \mathbf{h}, \boldsymbol{\beta}, \sigma^2) p(\mathbf{h}, \boldsymbol{\beta}, \sigma^2) d\mathbf{h} d\boldsymbol{\beta} d\sigma^2 \quad (3.11)$$

cannot be computed analytically. Hence, we decompose the full posterior distribution as

$$p(\mathbf{h}, \boldsymbol{\beta}, \sigma^2 | \mathbf{y}) \equiv p(\mathbf{h} | \mathbf{y}, \boldsymbol{\beta}, \sigma^2) p(\boldsymbol{\beta}, \sigma^2 | \mathbf{y}). \quad (3.12)$$

In (3.7), the noise term \mathbf{z} can be modeled probabilistically as independent zero-mean Gaussian random variables:

$$p(\mathbf{z}) = \prod_{m=1}^M \mathcal{N}(z_m | 0, \sigma^2). \quad (3.13)$$

This noise model infers Gaussian likelihood for observation \mathbf{y} :

$$p(\mathbf{y} | \mathbf{h}, \sigma^2) = (2\pi\sigma^2)^{-M/2} \exp\left(-\frac{\|\mathbf{y} - \Phi\mathbf{h}\|^2}{2\sigma^2}\right). \quad (3.14)$$

Since a Gaussian likelihood is inferred by AWGN term \mathbf{z} , a conjugate⁴ prior distribution has to be defined for computational convenience [49] so that the associated Bayesian inference may be performed in closed form [50]. Therefore, suppose that a zero-mean Gaussian prior distribution is defined on channel coefficients with $\{\beta_n\}$:

$$\begin{aligned} p(\mathbf{h} | \boldsymbol{\beta}) &= \prod_{n=1}^N \mathcal{N}(h_n | 0, \beta_n^{-1}) \\ &= (2\pi)^{-N/2} \prod_{n=1}^N \beta_n^{1/2} \exp\left(-\frac{\beta_n h_n^2}{2}\right). \end{aligned} \quad (3.15)$$

³For the implementation of BCS, the codes provided by Shihao Ji publicly available at <http://people.ee.duke.edu/~lcarin/BCS.html> are used.

⁴In Bayesian probability theory, a class of prior probability distributions $p(\boldsymbol{\theta})$ is said to be conjugate to a class of likelihood functions $p(\mathbf{y} | \boldsymbol{\theta})$ if the resulting posterior distributions $p(\boldsymbol{\theta} | \mathbf{y})$ are in the same family as $p(\boldsymbol{\theta})$ [50].

$\{\beta_n\}$'s are independent hyperparameters that form the $\boldsymbol{\beta} = [\beta_1, \dots, \beta_N]^T$ vector and control the strength of the prior over associated channel coefficients individually.

The first term of (3.12), $p(\mathbf{h} | \mathbf{y}, \boldsymbol{\beta}, \sigma^2)$, the posterior distribution over the channel coefficients, can be expressed via Bayes' rule as

$$p(\mathbf{h} | \mathbf{y}, \boldsymbol{\beta}, \sigma^2) = \frac{p(\mathbf{y} | \mathbf{h}, \sigma^2) p(\mathbf{h} | \boldsymbol{\beta})}{p(\mathbf{y} | \boldsymbol{\beta}, \sigma^2)}. \quad (3.16)$$

Considering Gaussian likelihood together with Gaussian prior, this posterior distribution is also $\mathcal{N}(\boldsymbol{\mu}, \boldsymbol{\Sigma})$ where

$$\begin{aligned} \boldsymbol{\Sigma} &= (\boldsymbol{\Lambda} + \sigma^{-2} \boldsymbol{\Phi}^T \boldsymbol{\Phi})^{-1}, \\ \boldsymbol{\mu} &= \sigma^{-2} \boldsymbol{\Sigma} \boldsymbol{\Phi}^T \mathbf{y}, \end{aligned} \quad (3.17)$$

with $\boldsymbol{\Lambda} = \text{diag}(\beta_1, \beta_2, \dots, \beta_N)$ and is analytically tractable. To compute the full posterior distribution approximately, hyperparameter posterior $p(\boldsymbol{\beta}, \sigma^2 | \mathbf{y})$, the second term in (3.12), needs to be approximated. This approximation is provided by type-II ML procedure. This procedure, also known as the evidence approximation or the empirical Bayes, is used to estimate hyperparameters by maximizing the marginal likelihood function (LF) [51, 52]. According to the Bayes' theorem, hyperparameter posterior $p(\boldsymbol{\beta}, \sigma^2 | \mathbf{y})$ can be expressed as:

$$p(\boldsymbol{\beta}, \sigma^2 | \mathbf{y}) \propto p(\mathbf{y} | \boldsymbol{\beta}, \sigma^2) p(\boldsymbol{\beta}, \sigma^2). \quad (3.18)$$

Using appropriately selected uniform⁵ hyperpriors for $\boldsymbol{\beta}$ and σ^2 in (3.18) (*i.e.*, $p(\boldsymbol{\beta}, \sigma^2 | \mathbf{y}) \propto p(\mathbf{y} | \boldsymbol{\beta}, \sigma^2)$), the estimates of $\boldsymbol{\beta}$ and σ^2 can be found by maximizing marginal LF $p(\mathbf{y} | \boldsymbol{\beta}, \sigma^2)$ as a consequence of type-II ML procedure. The marginal LF can be obtained by integrating over the channel coefficients \mathbf{h} as:

$$p(\mathbf{y} | \boldsymbol{\beta}, \sigma^2) = \int_{-\infty}^{\infty} p(\mathbf{y} | \mathbf{h}, \sigma^2) p(\mathbf{h} | \boldsymbol{\beta}) d\mathbf{h}. \quad (3.19)$$

Maximization of the marginal LF with respect to $\boldsymbol{\beta}$ or equivalently, its logarithm can be expressed as:

$$\begin{aligned} \mathcal{L}(\boldsymbol{\beta}, \sigma^2) &= \log p(\mathbf{y} | \boldsymbol{\beta}, \sigma^2) \\ &= \log \int_{-\infty}^{\infty} p(\mathbf{y} | \mathbf{h}, \sigma^2) p(\mathbf{h} | \boldsymbol{\beta}) d\mathbf{h} \\ &= -\frac{1}{2} [M \log(2\pi) + \log |\mathbf{C}| + \mathbf{y}^T \mathbf{C}^{-1} \mathbf{y}] \end{aligned} \quad (3.20)$$

⁵Uniform or flat hyperpriors are known as noninformative hyperpriors [49] which have a minimum effect on the hyperparameter posterior and they can be ignored.

where $\mathbf{C} = \sigma^2 \mathbf{I} + \Phi \Lambda^{-1} \Phi^T$ and $\mathbf{I} \in \mathfrak{R}^{M \times M}$ is an identity matrix. Differentiating $\mathcal{L}(\boldsymbol{\beta}, \sigma^2)$ with respect to $\boldsymbol{\beta}$ and σ^2 , and equating it to zero yields the following expressions which can be solved iteratively [29]:

$$\beta_n^{new} = \frac{\gamma_n}{\mu_n^2}, \quad \sigma^{2new} = \frac{\|\mathbf{y} - \Phi \boldsymbol{\mu}\|_2^2}{M - \sum_{n=1}^N \gamma_n}, \quad (3.21)$$

where $\gamma_n \in [0, 1]$ is defined as $\gamma_n = 1 - \beta_n \sum_{nn}$ with \sum_{nn} being the n th diagonal element of the posterior coefficient covariance from (3.17) and μ_n is the n th posterior coefficient mean from (3.17).

By employing re-estimates of hyperparameters, an iterative systematic approach is used to determine which basis vectors should be included in the model and which should be removed to promote sparsity [30].

After presenting the theories of applications of ℓ_1 -norm minimization and BCS to the UWB channel estimation, estimation of a CM-1 channel realization (CM-1 has the sparsest structure among the channel models considered, see Figure 2.9) with both ℓ_1 -norm minimization and BCS when the SNR level is at 5dB and 20dB are given in Figures 3.2 and 3.3, respectively. For the implementation of CM-1, channel length of $T_c = 100\text{ns}$ and channel resolution of $T_s = 0.25\text{ns}$ are adequate to take into account all multipaths and to resolve these multipaths individually. The corresponding discrete time channel length becomes $N = T_c/T_s = 400$. The number of measurements used for the estimation is $M = 200$. To remove the path loss effect, the channel coefficients are normalized as $\sum_{n=1}^N c_n^2 = 1$.

When the Figures 3.2 and 3.3 are compared, it is seen that the estimation performance of ℓ_1 -norm minimization is superior than BCS at 5dB SNR level. The two estimation error values (ℓ_1 -norm minimization error = 0.4731, BCS error = 1.0976) of the channel coefficients vector for ℓ_1 -norm minimization and BCS justifies this argument. On the other hand for 20dB SNR level, the estimation performance of BCS is superior than ℓ_1 -norm minimization. Similarly, this argument can be justified with the estimation error values (ℓ_1 -norm minimization error = 0.0578, BCS error = 0.0120) of the channel coefficients vector for both methods. Unlike the ℓ_1 -norm minimization, BCS uses prior distribution of the channel coefficients (thereby posterior distribution over channel coefficients) for the estimation. Due to the destructive effects of the noise at

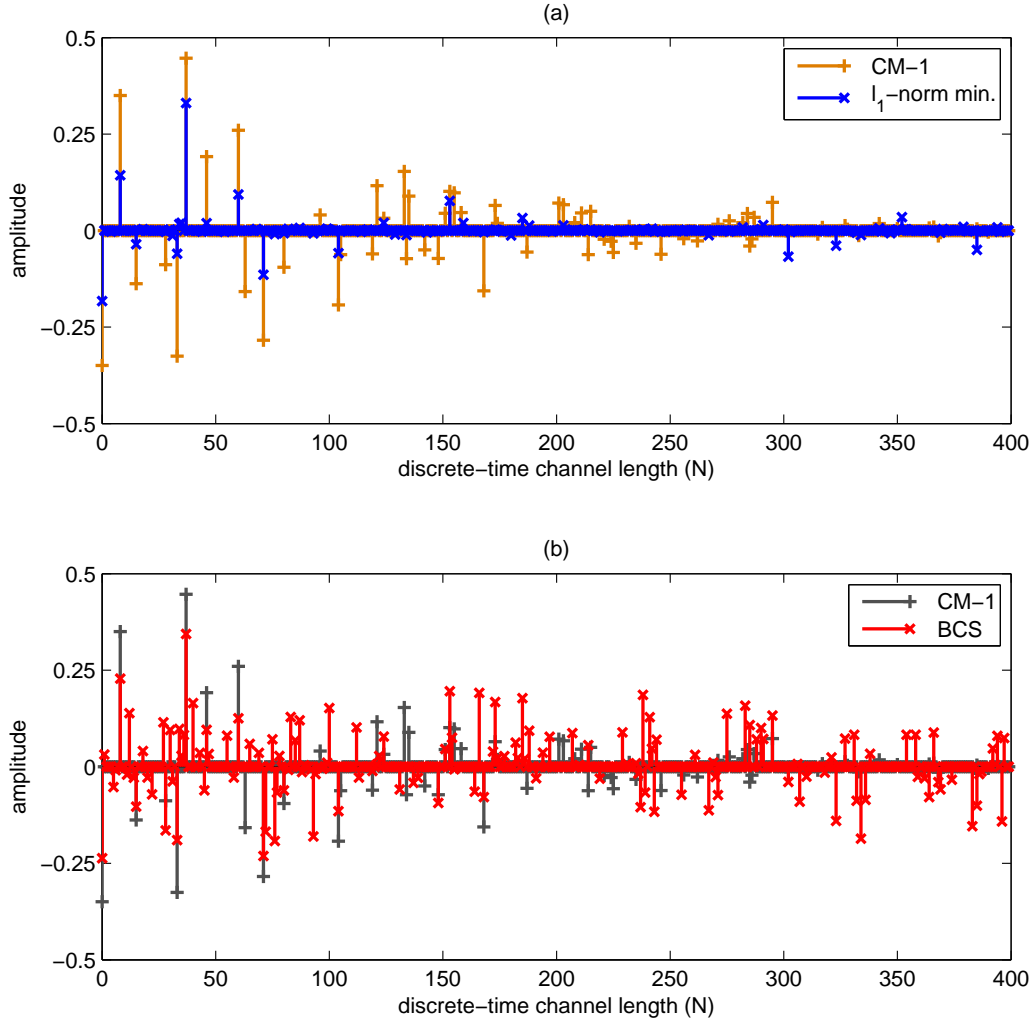


Figure 3.2 : Estimation of a CM-1 signal with ℓ_1 -norm minimization and BCS when $T_c = 100\text{ns}$, $T_s = 0.25\text{ns}$, $N = 400$, $M = 200$ and $\text{SNR} = 5\text{dB}$. **(a)** A CM-1 signal and its estimation with ℓ_1 -norm minimization, estimation error of the channel coefficients vector for ℓ_1 -norm minimization = 0.4731; **(b)** Same CM-1 signal in (a) and its estimation with BCS, estimation error of the channel coefficients vector for BCS = 1.0976.

low SNR (i.e., when the domination of the noise is increased), BCS cannot attain an accurate prior information about the coefficients. Therefore at 5dB SNR level, BCS estimates paths at non-path locations indeed. On the other hand, destructive effects of the noise is decreased significantly at 20 dB SNR level and with the accurate prior information, estimation performance of the BCS becomes superior than the performance of ℓ_1 -norm minimization. It can be concluded from this estimation example that BCS has a superior performance compared to ℓ_1 -norm minimization at

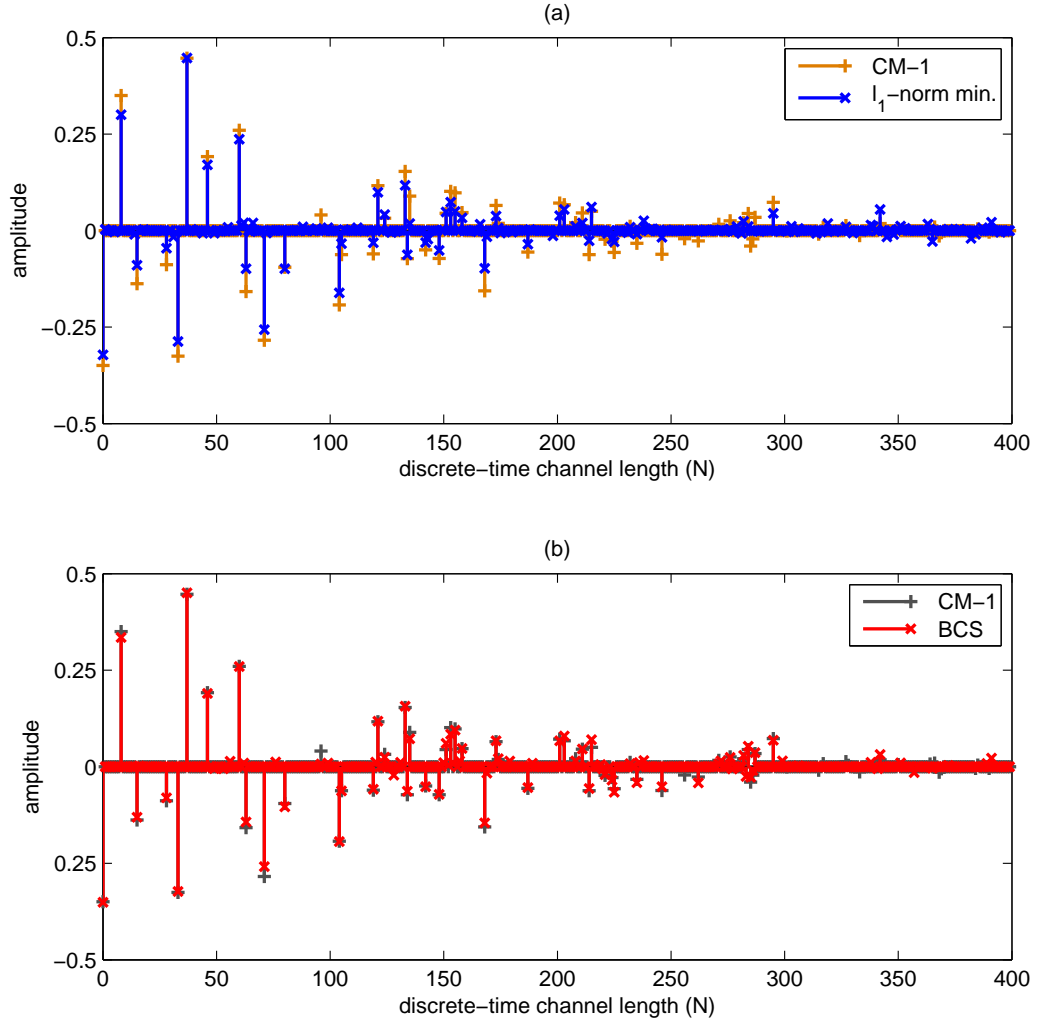


Figure 3.3 : Estimation of the same CM-1 signal in Figure 3.2 with ℓ_1 -norm minimization and BCS when $T_c = 100\text{ns}$, $T_s = 0.25\text{ns}$, $N = 400$, $M = 200$ and $\text{SNR} = 20\text{dB}$. **(a)** Same CM-1 signal and its estimation with ℓ_1 -norm minimization, estimation error of the channel coefficients vector for ℓ_1 -norm minimization = 0.0578; **(b)** Same CM-1 signal in (a) and its estimation with BCS, estimation error of the channel coefficients vector for BCS = 0.0120.

higher SNR regions. The detailed analysis for the effect of SNR regions on the channel estimation performance will be given in the Results chapter.

Beside the application of BCS to the UWB channel estimation, also an MSE performance lower bound is provided for *biased* BCS based channel estimator. The evaluation of this bound is given in the next chapter.

4. PERFORMANCE ANALYSIS

As in any estimation application, it is useful to quantify the best performance that may be achieved from channel estimator approach proposed. Performance bounds can serve as a benchmark with the goal of facilitating performance comparisons of the various estimation techniques under consideration. Such bounds may also indicate characteristics of the problem that require extra attention for optimal performance.

The CRLB is a widely used performance bound in order to indicate the minimum achievable total variance of any *unbiased* estimator of deterministic parameter vector [36]. Since MSE becomes equal to variance for *unbiased* (zero bias) estimators, CRLB also provides a benchmark on the estimation error for this type of estimators. However, the BCS estimator proposed for UWB channel estimation in this study is a *biased* estimator as well as being Bayesian. Accordingly, restriction to *unbiased* approach of the lower bound for the problem at hand leads to unreasonable performance results. It is necessary to determine a lower bound on the estimation error which characterizes both the total variance and the bias of the *biased* estimator. Hence, an MSE lower bound for *biased* Bayesian estimators ($MSE_{l,b}$, where subscript l stands for lower bound and subscript b stands for *biased* Bayesian) is provided by making use of bound in [37], which is based on *biased* CRLB in [53]. In literature, PCRLB or Bayesian CRLB [35] was defined for *unbiased* Bayesian estimators considering prior information about the parameter vector that is wanted to estimate. In addition to CRLB, PCRLB also takes into account prior probability distribution of the parameter vector. Nevertheless, PCRLB is a lower bound on the variance of the *unbiased* Bayesian estimator not on the estimation error. Accordingly, the $MSE_{l,b}$ that is provided considering bias with the prior information of channel vector will become a lower bound on the estimation error of *biased* Bayesian estimators. Note that the bias and the prior distribution of the parameter vector are included in the derivation of the performance bound presented below, however, the sparsity conditions are not

incorporated into the model and are subject for future research. The MSE of *general* and *Bayesian* biased estimators are presented in the following sections, respectively.

4.1 MSE of a Biased Estimator

In what follows, MSE of the *biased* estimator is expressed as a sum of the squared norm of bias and trace of covariance matrix for the channel vector \mathbf{h} with given linear signal model in (3.7),

$$MSE(\hat{\mathbf{h}}_b) = E \left\{ \|\hat{\mathbf{h}}_b - \mathbf{h}\|^2 \right\} = \|b(\mathbf{h})\|^2 + Tr(\mathbf{C}_{\hat{\mathbf{h}}_b}), \quad (4.1)$$

where bias vector, $b(\mathbf{h}) \in \mathfrak{R}^N$, and covariance matrix of the *biased* estimator, $\mathbf{C}_{\hat{\mathbf{h}}_b} \in \mathfrak{R}^{N \times N}$, can be denoted respectively as

$$b(\mathbf{h}) = E \{ \hat{\mathbf{h}}_b \} - \mathbf{h}, \quad (4.2)$$

$$\mathbf{C}_{\hat{\mathbf{h}}_b} = E \left\{ [\hat{\mathbf{h}}_b - E(\hat{\mathbf{h}}_b)] [\hat{\mathbf{h}}_b - E(\hat{\mathbf{h}}_b)]^T \right\}, \quad (4.3)$$

and $\hat{\mathbf{h}}_b \in \mathfrak{R}^N$ corresponds to estimated channel vector.

Regarding suitability of regularity condition on $p(\mathbf{y} | \mathbf{h})$ [36]

$$E_{\mathbf{y}} \left[\frac{\partial \ln p(\mathbf{y} | \mathbf{h})}{\partial \mathbf{h}} \right] = 0 \quad \forall \mathbf{h}, \quad (4.4)$$

biased CRLB in [53] for any *biased* estimator with a given bias can be obtained for the vector case as follows:

$$\text{Cov}(\hat{\mathbf{h}}_b) \geq \frac{\left(1 + \frac{\partial b(\mathbf{h})}{\partial \mathbf{h}}\right)^2}{E_{\mathbf{y}|\mathbf{h}} \left\{ \left[\frac{\partial \ln p_{\mathbf{y}|\mathbf{h}}(\mathbf{y}|\mathbf{h})}{\partial \mathbf{h}} \right]^T \left[\frac{\partial \ln p_{\mathbf{y}|\mathbf{h}}(\mathbf{y}|\mathbf{h})}{\partial \mathbf{h}} \right] \right\}}, \quad (4.5)$$

where the denominator of (4.5) also can be denoted as

$$E_{\mathbf{y}|\mathbf{h}} \left\{ \left[\frac{\partial \ln p_{\mathbf{y}|\mathbf{h}}(\mathbf{y}|\mathbf{h})}{\partial \mathbf{h}} \right]^T \left[\frac{\partial \ln p_{\mathbf{y}|\mathbf{h}}(\mathbf{y}|\mathbf{h})}{\partial \mathbf{h}} \right] \right\} = -E_{\mathbf{y}|\mathbf{h}} \left\{ \left[\frac{\partial^2 \ln p_{\mathbf{y}|\mathbf{h}}(\mathbf{y}|\mathbf{h})}{\partial \mathbf{h}^T \partial \mathbf{h}} \right] \right\}. \quad (4.6)$$

4.2 MSE of Bayesian Biased Estimator

Counterpart of the *biased* CRLB in Bayesian framework can be expressed for Bayesian estimators as

$$\mathbf{C}_{\hat{\mathbf{h}}_b} = \text{Cov}(\hat{\mathbf{h}}_b) \geq \frac{\left(1 + \frac{\partial b(\mathbf{h})}{\partial \mathbf{h}}\right)^2}{-E_{\mathbf{y},\mathbf{h}} \left\{ \left[\frac{\partial^2 \ln p_{\mathbf{y},\mathbf{h}}(\mathbf{y},\mathbf{h})}{\partial \mathbf{h}^T \partial \mathbf{h}} \right] \right\}}. \quad (4.7)$$

Moreover, the denominator of (4.7) can be decomposed into two parts using the Bayes' rule:

$$-E_{\mathbf{y},\mathbf{h}} \left\{ \left[\frac{\partial^2 \ln p_{\mathbf{y},\mathbf{h}}(\mathbf{y}, \mathbf{h})}{\partial \mathbf{h}^T \partial \mathbf{h}} \right] \right\} = -E_{\mathbf{y}|\mathbf{h}} \left\{ \left[\frac{\partial^2 \ln p_{\mathbf{y}|\mathbf{h}}(\mathbf{y}|\mathbf{h})}{\partial \mathbf{h}^T \partial \mathbf{h}} \right] \right\} - E_{\mathbf{h}} \left\{ \left[\frac{\partial^2 \ln p_{\mathbf{h}}(\mathbf{h})}{\partial \mathbf{h}^T \partial \mathbf{h}} \right] \right\} \quad (4.8)$$

which can be expressed in matrix form as

$$\mathbf{J}_H = \mathbf{J}_D + \mathbf{J}_P, \quad (4.9)$$

where $\mathbf{J}_H \in \mathfrak{R}^{N \times N}$, $\mathbf{J}_D \in \mathfrak{R}^{N \times N}$ and $\mathbf{J}_P \in \mathfrak{R}^{N \times N}$ correspond to Bayesian Fisher information matrix (FIM), observation data (\mathbf{y}) information matrix and prior information matrix, respectively. Considering the linear signal model in (3.7) with (3.13) and (3.14), observation data information matrix \mathbf{J}_D can be expressed as

$$\mathbf{J}_D = -E_{\mathbf{y}|\mathbf{h}} \left\{ \left[\frac{\partial^2 \ln p_{\mathbf{y}|\mathbf{h}}(\mathbf{y}|\mathbf{h})}{\partial \mathbf{h}^T \partial \mathbf{h}} \right] \right\} = \mathbf{A}^T \mathbf{C}_z^{-1} \mathbf{A}, \quad (4.10)$$

where $\mathbf{C}_z = \sigma^2 \mathbf{I} \in \mathfrak{R}^{M \times M}$ is the covariance matrix of the noise term \mathbf{z} and $\mathbf{A} \in \mathfrak{R}^{M \times N}$ is the measurement matrix which is also a full rank matrix. Exploiting assumption ($\mathbf{h} \sim \mathcal{N}(0, \mathbf{C}_h)$) in (3.15), prior information matrix \mathbf{J}_P is equal to inverse of covariance matrix of the channel vector $\mathbf{C}_h \in \mathfrak{R}^{N \times N}$:

$$\mathbf{J}_P = -E_{\mathbf{h}} \left\{ \frac{\partial^2 \ln p_{\mathbf{h}}(\mathbf{h})}{\partial \mathbf{h}^T \partial \mathbf{h}} \right\} = \mathbf{C}_h^{-1}. \quad (4.11)$$

\mathbf{C}_h is a diagonal matrix and each diagonal element is formed by inverse of the hyperparameters

$$\mathbf{C}_h = \text{diag} \{ \beta_n^{-1} \}, \quad n \in \{1, 2, \dots, N\}. \quad (4.12)$$

Once \mathbf{J}_D and \mathbf{J}_P are obtained, the Bayesian FIM \mathbf{J}_H can be rewritten in compact form as

$$\mathbf{J}_H = (\mathbf{A}^T \mathbf{C}_z^{-1} \mathbf{A}) + \mathbf{C}_h^{-1}. \quad (4.13)$$

Since the denominator of (4.7) is obtained, to form a final expression for the *biased* Bayesian CRLB, an a-priori choice of the bias gradient is required. In [37], estimators with only linear bias vectors are considered instead of taking into account all possible estimators. For its simplicity and tractability, only linear bias vectors are also considered in this study. Advantages of restricting attention to linear bias vectors can

be expressed as follows. Linear bias case is easier than nonlinear cases analytically and it is also easy to constitute estimators achieving the corresponding MSE lower bound with the efficient unbiased estimators practically [37]. Linear bias vector can be denoted as

$$b(\mathbf{h}) = \mathbf{S}\mathbf{h}, \quad (4.14)$$

where $\mathbf{S} \in \mathfrak{R}^{N \times N}$ is the bias gradient matrix defined by

$$\mathbf{S} = \frac{\partial b(\mathbf{h})}{\partial \mathbf{h}}. \quad (4.15)$$

Thus, (4.7) can be rearranged as

$$\mathbf{C}_{\hat{\mathbf{h}}_b} \geq (\mathbf{I} + \mathbf{S}) \mathbf{J}_H^{-1} (\mathbf{I} + \mathbf{S})^T, \quad (4.16)$$

where $\mathbf{I} \in \mathfrak{R}^{N \times N}$ is an identity matrix. Inserting (4.14) and (4.16) into (4.1), the $MSE_{l,b}$ for *biased* Bayesian estimators can be obtained as

$$\begin{aligned} MSE_{l,b} &= E \left\{ \|\hat{\mathbf{h}}_b - \mathbf{h}\|^2 \right\} \\ &= \mathbf{h}^T \mathbf{S}^T \mathbf{S} \mathbf{h} + Tr \left\{ (\mathbf{I} + \mathbf{S}) \mathbf{J}_H^{-1} (\mathbf{I} + \mathbf{S})^T \right\}. \end{aligned} \quad (4.17)$$

Now, the optimal \mathbf{S} matrix needs to be determined to find the achievable smallest MSE over all estimators with linear bias. Since (4.17) is convex in \mathbf{S} , the smallest value of $MSE_{l,b}$ can be found by equating its derivative to zero

$$\begin{aligned} \frac{\partial \mathbf{h}^T \mathbf{S}^T \mathbf{S} \mathbf{h} + Tr \left\{ (\mathbf{I} + \mathbf{S}) \mathbf{J}_H^{-1} (\mathbf{I} + \mathbf{S})^T \right\}}{\partial \mathbf{S}} &= 0 \\ 2\mathbf{h}^T \mathbf{h} \mathbf{S} + 2\mathbf{J}_H^{-1} + 2\mathbf{J}_H^{-1} \mathbf{S} &= 0, \end{aligned} \quad (4.18)$$

which yields

$$\mathbf{S}(\mathbf{J}_H^{-1} + \mathbf{h}^T \mathbf{h}) = -\mathbf{J}_H^{-1}. \quad (4.19)$$

Multiplying both sides of (4.19) with $(\mathbf{J}_H^{-1} + \mathbf{h}^T \mathbf{h})^{-1}$ leaves the matrix \mathbf{S} alone at the left side in (4.19). Using the matrix inversion lemma in (4.20) with the replacements of $\mathbf{D} = \mathbf{J}_H^{-1}$, $\mathbf{U} = \mathbf{h}^T$, $\mathbf{Q} = \mathbf{I}$, $\mathbf{V} = \mathbf{h}$

$$(\mathbf{D} + \mathbf{U}\mathbf{Q}\mathbf{V})^{-1} = \mathbf{D}^{-1} - \mathbf{D}^{-1}\mathbf{U}(\mathbf{Q}^{-1} + \mathbf{V}\mathbf{D}^{-1}\mathbf{U})^{-1}\mathbf{V}\mathbf{D}^{-1}, \quad (4.20)$$

$(\mathbf{J}_H^{-1} + \mathbf{h}^T \mathbf{h})^{-1}$ can be expressed as

$$(\mathbf{J}_H^{-1} + \mathbf{h}^T \mathbf{h})^{-1} = \mathbf{J}_H - \frac{\mathbf{J}_H \mathbf{h} \mathbf{h}^T \mathbf{J}_H}{1 + \mathbf{h}^T \mathbf{J}_H \mathbf{h}}. \quad (4.21)$$

After multiplying the right side of (4.19) with (4.21), the optimal \mathbf{S} matrix can be obtained as follows:

$$\mathbf{S} = -\mathbf{I} + \frac{1}{1 + \mathbf{h}^T \mathbf{J}_H \mathbf{h}} \mathbf{h} \mathbf{h}^T \mathbf{J}_H. \quad (4.22)$$

Note that when $\mathbf{S} = 0$, which is the zero bias case, CRLB for *unbiased* Bayesian estimators (i.e., PCRLB) is obtained: $MSE_{l,b} = Tr(\mathbf{J}_H^{-1})$. Therefore $MSE_{l,b}$ also includes *unbiased* Bayesian estimation as a special case.

The results of the $MSE_{l,b}$ provided in this chapter together with detailed analysis of the effects of noise level, number of measurements and sparsity are given in the following chapter.

5. RESULTS

The numerical results of the application of BCS to the UWB channel estimation is composed of two sections, as follows:

(a) *performance results section*, which includes the channel estimation performance of BCS for various UWB channel models, noise conditions and number of measurements compared to the results of ℓ_1 -norm minimization based estimation and MSE lower bounds of BCS performances, and

(b) *computation efficiency section*, which includes the comparison of computation efficiencies of BCS and ℓ_1 -norm minimization in terms of computation times.

5.1 Performance Results

In this section, the effects of (i) number of measurements, (ii) SNR regions, and (iii) the IEEE 802.15.4a channel models on the BCS channel estimation performance are investigated, and the results are compared to the performance of the ℓ_1 -norm minimization results. Furthermore, MSE lower bounds for the BCS performances in the channel models are provided. As the performance measure, the MSE of the estimated channel vector is evaluated. To remove the path loss effect and to treat each channel model fairly, the channel coefficients are normalized as $\sum_{n=1}^N c_n^2 = 1$. For the simulations, the channel length and resolution are fixed to $T_c = 250\text{ns}$ and $T_s = 0.25\text{ns}$, respectively, resulting in the discrete-time channel length $N = T_c/T_s = 1000$. The elements of the measurement matrix Φ are obtained from the $\mathcal{N}(0,1)$ distribution, and the basis where the channel vector is sparse is defined as $\Psi = \mathbf{I}$ in the simulations.

5.1.1 Effect of number of measurements on the MSE performance

In Figure 5.1, MSE performances of ℓ_1 -norm minimization and BCS are compared with respect to number of measurements (M) at 20dB SNR level. Here, M/N can be regarded as the compression ratio (i.e., the ratio of number of measurements to

the length of the equivalent discrete-time channel). As expected, BCS outperforms ℓ_1 -norm minimization in the sparser channel models (i.e., CM-1 and CM-2) for the number of measurements greater than $M = 110$ and $M = 160$, respectively, at 20dB. Due to the sparse structures of the CM-1 and CM-2, these number of measurements are adequate to outperform ℓ_1 -norm minimization. For these channel models, MSE performances of both estimation methods do not change much with the number of measurements between $600 < M < 750$. Hence, the number of measurements can be limited with $M = 600$. It means that the required sampling rate for minimum MSE can be decreased for CM-1 and CM-2 with negligible MSE performance degradation.

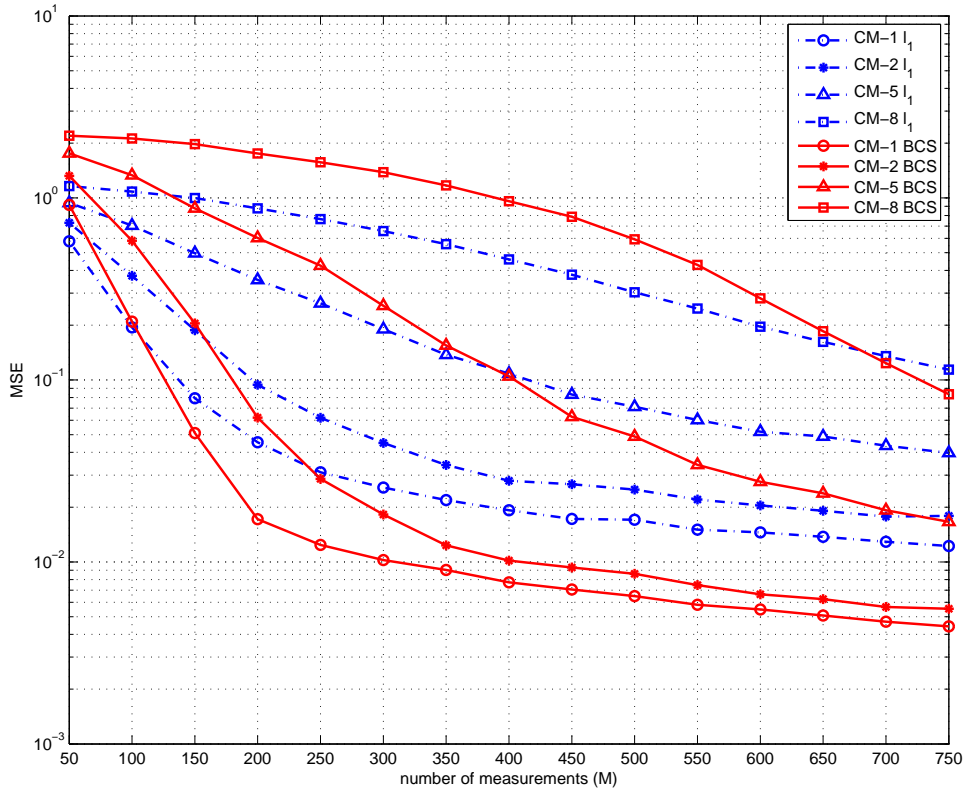


Figure 5.1 : Effect of the number of measurements on the MSE performances of BCS and ℓ_1 -norm minimization estimations for the channel models when $SNR = 20\text{dB}$.

For CM-5, BCS has a superior MSE performance for the number of measurements greater than $M = 380$. The goal here is to achieve the channel estimation with minimum MSE and maximum compression ratio (minimum number of measurements). As the sparsity decreases for CM-5 in comparison with CM-1 and

CM-2, more number of measurements are needed in order for BCS to outperform ℓ_1 -norm minimization. Accordingly, the compression ratio decreases for BCS in CM-5. For CM-8, which is not a sparse channel model, the number of measurements should be greater than $M = 680$ in order for BCS to have a superior performance compared to ℓ_1 -norm minimization. Therefore, the minimum compression ratio among the channel models for BCS is acquired for CM-8. As a result, it is seen from Figure 5.1 that superior MSE performances are obtained with BCS compared to ℓ_1 -norm minimization with significantly fewer measurements in CM-1 and CM-2, which are the sparser channel models, than required in CM-5 and CM-8, which have less sparse structures.

5.1.2 Effect of channel models on the MSE performance and MSE lower bounds

The performances are evaluated for $M = \{250, 500, 750\}$ measurements in the $[0, 30]$ dB SNR region in this part of the chapter. In Figures 5.2, 5.3, 5.4 and 5.5, the channel estimation performances of BCS and ℓ_1 -norm minimization are compared for various number of measurements and SNR values for the channel models CM-1, CM-2, CM-5 and CM-8, respectively. The best channel estimation performance for both methods is obtained for CM-1, as it exhibits the sparsest structure among these channel models (see Figure 2.9 and Table 2.1). BCS outperforms ℓ_1 -norm minimization in the sparser channel models CM-1 and CM-2 for SNR values greater than 12-13dB for all measurements considered. This can be explained as for the higher SNR regions posterior density function over the channel coefficients and noise is beneficial to the channel coefficients estimation, whereas for lower SNR regions the uncertainty in the estimation is higher. As for CM-5, which is a less sparse channel, the number of measurements should be greater than $M = 500$ in order for BCS to have a superior performance at higher SNR regions. As for CM-8, which is not a sparse channel model, as the multipaths arrive almost in every time bin, the BCS performs inferior compared to the ℓ_1 -norm minimization for almost all conditions. In summary, BCS can be an effective channel estimation method for sparser channel models at high SNR regions. This is mainly due to BCS considering the channel and noise statistics

and providing a posterior density function over noise and the channel coefficients, whereas the ℓ_1 -norm minimization method not utilizing such statistics.

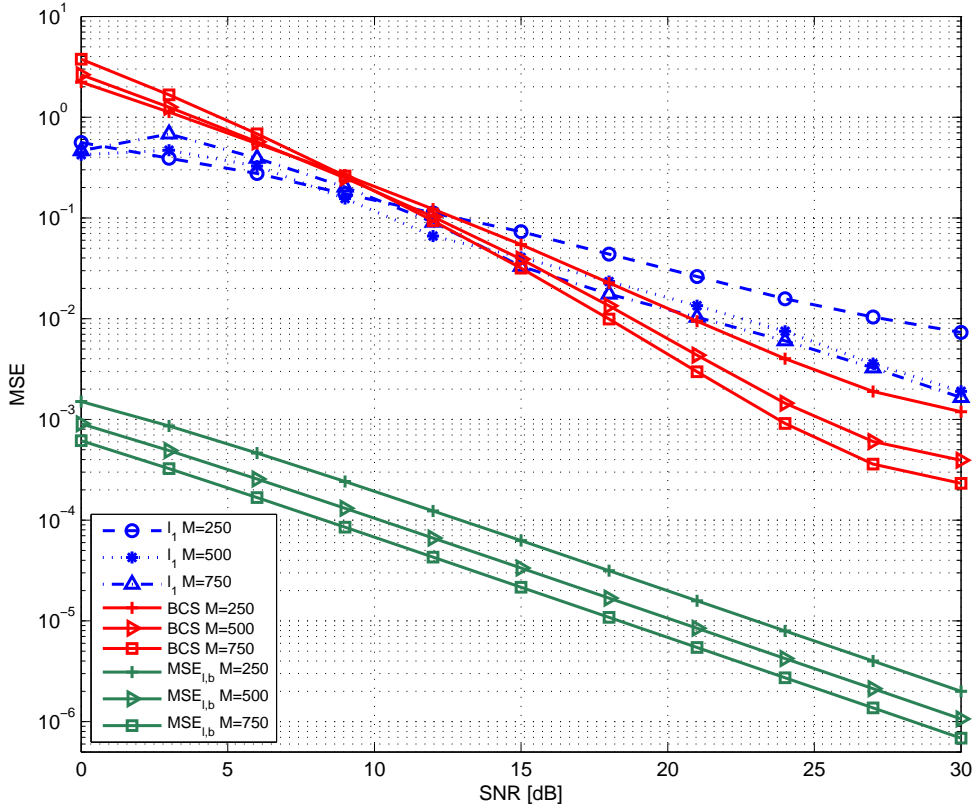


Figure 5.2 : MSE performance comparison of BCS and ℓ_1 -norm minimization for CM-1.

The MSE performance results with respect to the number of measurements given in Figure 5.1 are consistent with the results for $SNR = 20\text{dB}$ given in figures in this section.

Next, the MSE performance of BCS is compared with the MSE lower bound, $MSE_{l,b}$, in Figures 5.2, 5.3, 5.4 and 5.5. It can be observed that the MSE lower bound performance improves with the number of measurements M as expected. On the other hand, for M fixed the MSE bounds are similar for different channel models. This can be explained as follows. When quantified, the $MSE_{l,b}$ term in (4.17) is observed to be dominated by the second term, which depends on $\mathbf{J}_H = \mathbf{J}_D + \mathbf{J}_P$. Here, the observation data information matrix \mathbf{J}_D has more significant contribution compared to the prior information matrix \mathbf{J}_P that carries the channel model information. Therefore, $MSE_{l,b}$ values have found to be similar despite channel model differences. Lastly,

a performance gap between the MSE performance of BCS and the MSE lower bound is observed as in [35], where they compared their proposed CS based block maximum-a-posteriori least mean squares (CS-BMAP-LMS) method to the Bayesian CRLB. A tighter bound for the implementation of BCS may be obtained if the sparsity knowledge of the channel can be incorporated into the lower bound computation and the linearly assumed bias vector can be generalized to cover nonlinear bias vectors. Both considerations are non-trivial to implement, however, are expected to provide tighter bounds and subject to further investigation.

In the next section, the second part of the results, which is related to computation times of both methods will be presented.

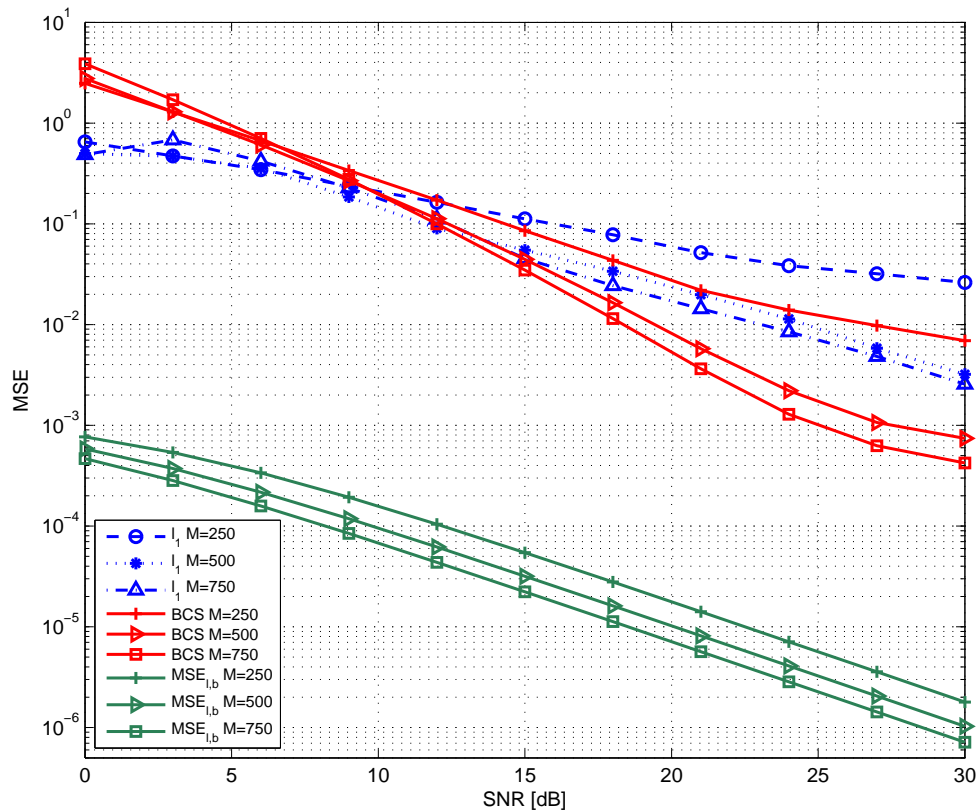


Figure 5.3 : MSE performance comparison of BCS and ℓ_1 -norm minimization for CM-2.

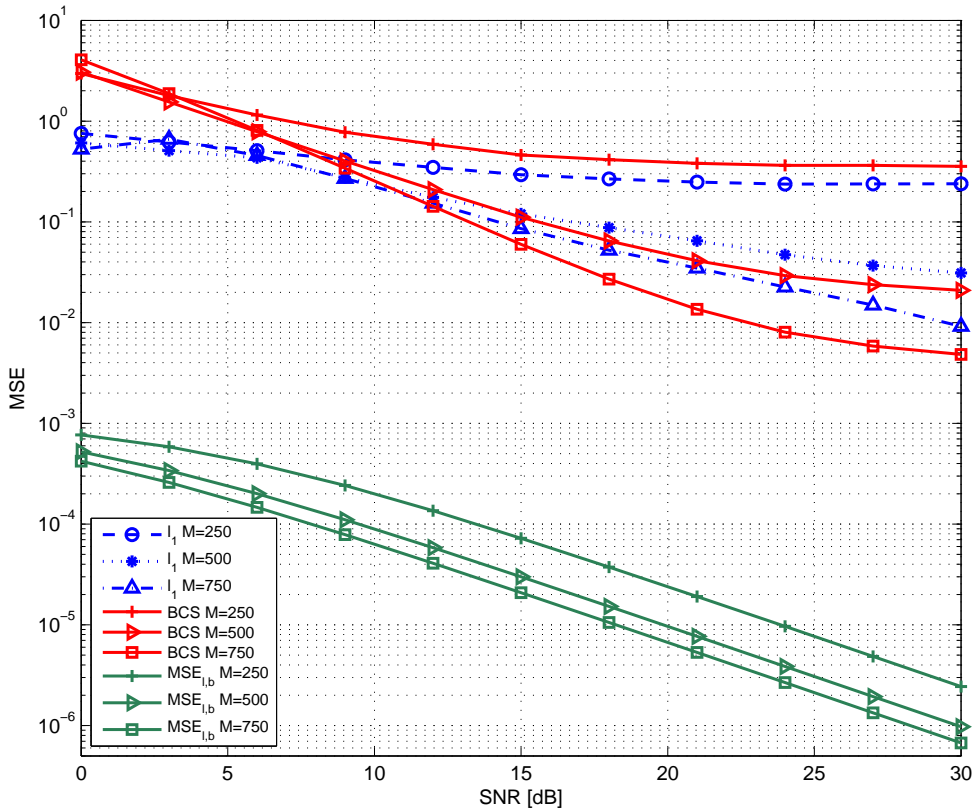


Figure 5.4 : MSE performance comparison of BCS and ℓ_1 -norm minimization for CM-5.

5.2 Computation Efficiency

Before presenting numerical values for computation times, a short discussion on the comparison of computation efficiencies of both BCS and ℓ_1 -norm minimization is provided in this section.

In ℓ_1 -norm minimization, whose computational complexity is proportional to $O(N^3)$ [54], the basis vectors are added to the model and never removed during the channel coefficients estimation. Therefore, not only the K basis vectors that correspond to nonzero coefficients but all basis vectors are considered during the channel estimation process. This situation apparently increases the computational complexity of this method. However, in BCS, whose computational complexity is proportional to $O(NK^2)$, there is an iterative update approach which sequentially adds or removes

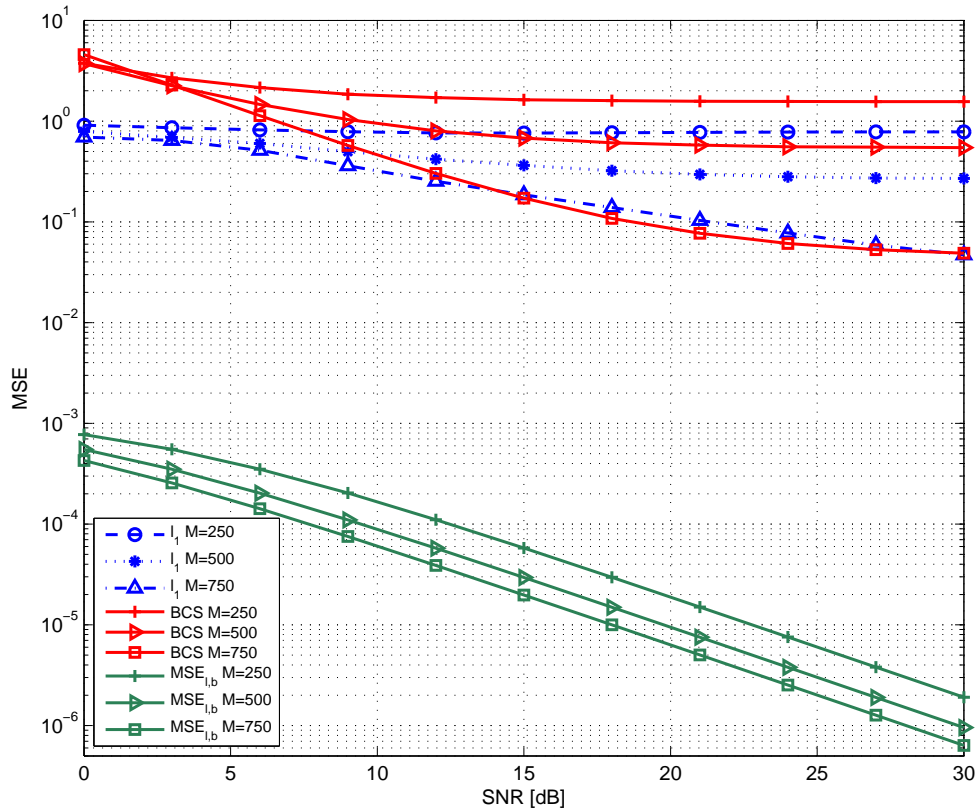


Figure 5.5 : MSE performance comparison of BCS and ℓ_1 -norm minimization for CM-8.

basis vectors to the model until all K basis vectors have been included [30]. Thus, BCS is computationally more efficient compared to the ℓ_1 -norm minimization.

To justify this argument, computation times of both methods are provided. The average computation times of the channel estimators for both methods are compared based on the publicly available codes, where their main structures are not modified but adapted to IEEE 802.15.4a channel estimation. In Tables 5.1, 5.2, 5.3 and 5.4, the computation times of both methods are presented for different number of measurements in CM-1, CM-2, CM-5 and CM-8, respectively. The simulations were run on a computer that has a 3.4 GHz Intel Core i7 CPU and a 3.88 GB RAM. It can be observed that the computation time of BCS is significantly shorter than the ℓ_1 -norm minimization for every channel model and number of observations. It can be further observed that the computation time of ℓ_1 -norm minimization does not change much with sparsity or the number of measurements. This can be explained by the computational complexity of ℓ_1 -norm minimization not depending on the number of nonzero coefficients (K)

but only on the discrete-time channel length (N), which is the same for all channel models considered. Unlike ℓ_1 -norm minimization, the computational complexity of BCS depends on K , and therefore, the computation time of BCS changes remarkably with sparsity and the number of measurements.

Table 5.1 : Computation times of both methods for CM-1.

| Number of measurements | ℓ_1 -norm minimization | Bayesian CS |
|------------------------|-----------------------------|--------------|
| M=250 | 3.5911 secs | 0.13607 secs |
| M=500 | 3.6684 secs | 0.2892 secs |
| M=750 | 3.5778 secs | 0.76564 secs |

Table 5.2 : Computation times of both methods for CM-2.

| Number of measurements | ℓ_1 -norm minimization | Bayesian CS |
|------------------------|-----------------------------|--------------|
| M=250 | 3.6073 secs | 0.15767 secs |
| M=500 | 3.627 secs | 0.31896 secs |
| M=750 | 3.4591 secs | 0.82328 secs |

Table 5.3 : Computation times of both methods for CM-5.

| Number of measurements | ℓ_1 -norm minimization | Bayesian CS |
|------------------------|-----------------------------|--------------|
| M=250 | 3.748 secs | 0.22791 secs |
| M=500 | 3.5745 secs | 0.47146 secs |
| M=750 | 3.2783 secs | 1.1099 secs |

Table 5.4 : Computation times of both methods for CM-8.

| Number of measurements | ℓ_1 -norm minimization | Bayesian CS |
|------------------------|-----------------------------|--------------|
| M=250 | 3.8257 secs | 0.27791 secs |
| M=500 | 4.0806 secs | 0.84026 secs |
| M=750 | 3.6359 secs | 1.9952 secs |

The computation times of both methods are summarized in Table 5.5 for different channel models when the number of measurements is fixed to $M = 250$. Considering CM-1, which has the sparsest structure, and CM-8, which has the least sparse structure among the channel models, the computation time of ℓ_1 -norm minimization in CM-8 increases 6.53% compared to CM-1 but for BCS this ratio becomes 104.24%. Similar observations were made for the cases $M = \{500, 750\}$. This remarkable increase in

the computation time of BCS is a result of its computational complexity depending on K . Nevertheless, BCS is computationally more efficient compared to ℓ_1 -norm minimization as shown with practical examples.

Table 5.5 : Computation times of both methods for channel models when $M = 250$.

| Channel model | ℓ_1 -norm min. $\sim O(N^3)$ | Bayesian CS $\sim O(NK^2)$ |
|---------------|--------------------------------------|-------------------------------|
| CM-1 | 3.5911 secs | 0.13607 secs |
| CM-2 | 3.6073 secs | 0.15767 secs |
| CM-5 | 3.748 secs | 0.22791 secs |
| CM-8 | 3.8257 secs | 0.27791 secs |

6. CONCLUSION AND FUTURE WORK

In this thesis, the application of Bayesian CS to UWB channel estimation was considered, and its channel estimation performance for various UWB channel models and noise conditions was studied. Specifically, the effects of the (i) sparse structure of standardized IEEE 802.15.4a channel models, (ii) SNR regions, and (iii) number of measurements on the BCS channel estimation performance are investigated, and they are compared with the results of the conventional ℓ_1 -norm minimization based estimation. Moreover, an MSE lower bound on the estimation error for *biased* Bayesian estimators with linear bias vectors is provided, and computational efficiencies of both BCS and ℓ_1 -norm minimization for channel estimation are compared.

The results of this study show that BCS exhibits superior performance at sparser channel models and higher SNR regions as it utilizes the statistics of channel coefficients and noise. Furthermore, the computational efficiency of BCS has been found to be significantly better than ℓ_1 -norm minimization for the cases considered. Based on the results of this study, the implementation conditions of BCS can be determined for practical cases.

While this study focused on the UWB channel estimation performance of BCS for the IEEE 802.15.4a standardization, the future work may be the incorporation of sparsity knowledge of the channel for a tighter MSE bound and improvement of the MSE performance of BCS (prevention of BCS from estimating paths at the locations of non-existent paths) at lower SNR regions by exploiting this sparsity knowledge of the channel.

REFERENCES

- [1] **Win, M. Z. and Scholtz, R. A.** (2000). Ultra-widebandwidth time-hopping spread-spectrum impulse radio for wireless multiple-access communications, *IEEE Transactions on Communications*, **48**, 679–691.
- [2] **Porcino, D. and Hirt, W.** (2003). Ultra-wideband radio technology: potential and challenges ahead, *IEEE Communications Magazine*, **41(7)**, 66–74.
- [3] **Singh, S., Liang, Q., Chen, D. and Sheng, Li** (2011). Sense through wall human detection using UWB radar, *EURASIP Journal on Wireless Communications and Networking*, **2011**:20.
- [4] **Vitebskiy, S., Carin, L., Ressler, M. A. and Le, F. H.** (1997). Ultra-wideband short-pulse ground-penetrating radar: simulation and measurement, *IEEE Transactions on Geoscience and Remote Sensing*, **35(3)**, 762–772.
- [5] **Jalilvand, M., Pancera, E., Xuyang, L., Zwick, T. and Wiesbeck, W.** (2011). A sparse synthetic aperture-based UWB medical imaging system, *Proceedings of the 6th German Microwave Conference (GeMIC)*, pp. 1–4.
- [6] **Venkatasubramanian, V., Peiguo, L. and Leung, H.** (2004). Chaos based UWB imaging radar for homeland security, *IEEE Conference on Cybernetics and Intelligent Systems*, pp. 351–355.
- [7] **Sakkila, L., Tatkeu, C., Boukour, F., El Hillali, Y. Rivenq, A. and Rouvean, J. M.** (2008). UWB radar system for road anti-collision application, *Proceedings of the 3rd International Conference on Information and Communication Technologies: From Theory to Applications (ICTTA)*, pp. 1–6.
- [8] **Takahara, H., Ohno, K. and Itami, M.** (2012). A study on UWB radar assisted by inter-vehicle communication for safety applications, *IEEE International Conference on Vehicular Electronics and Safety (ICVES)*, pp. 99–104.
- [9] **Zhang, J., Orlik, P. V., Sahinoglu, Z., Molisch, A.F. and Kinney, P.** (2009). UWB systems for wireless sensor networks, *Proceedings of the IEEE*, **97(2)**, 313–331.
- [10] **Katsuta, H., Takei, Y., Takizawa, K. and Ikegami, T.** (2012). Experiments of ultra wideband-based wireless body area networks with multi-nodes attached to body, *Proceedings of the 3rd International Conference on Medical Information and Communication Technology (ISMICT)*, pp. 1–4.

- [11] **Ghavami, M., Michael, L. B. and Kohno, R.** (2009). *Ultra Wideband Signals and Systems in Communication Engineering*, Wiltshire, UK, Wiley.
- [12] **Ross, G. F. and Scholtz, R. A.** (1973). Transmission and reception system for generating and receiving base-band duration pulse signals without distortion for short base-band pulse communication system, *U.S. Patent*, No: 3,728,632 dated 17.04.1973.
- [13] **IEEE** (2007). Standard for Information Technology - Telecommunications and Information Exchange Between Systems - Local and Metropolitan Area Networks - Specific Requirement Part 15.4: Wireless Medium Access Control (MAC) and Physical Layer (PHY) Specifications for Low-Rate Wireless Personal Area Networks (WPANs), *IEEE Std 802.15.4a-2007*.
- [14] **Lottici, V., D'Andrea, A. and Mengali, U.** (2002). Channel estimation for ultra-wideband communications, *IEEE Journal on Selected Areas in Communications*, **20(9)**, 1638–1645.
- [15] **Huang, L. and Ko, C. C.** (2004). Performance of maximum-likelihood channel estimator for UWB communications, *IEEE Communications Letters*, **8(6)**, 356–358.
- [16] **Candès, E. J., Romberg, J. and Tao, T.** (2006). Robust uncertainty principles: exact signal reconstruction from highly incomplete frequency information, *IEEE Transactions on Information Theory*, **52**, 489–509.
- [17] **Donoho, D. L.** (2006). Compressed sensing, *IEEE Transactions on Information Theory*, **52**, 1289–1306.
- [18] **Eldar, Y. C. and Kutyniok, G.** (2012). *Compressed Sensing: Theory and Applications*, New York, Cambridge University Press.
- [19] **Lampe, L. and Witrisal, K.** (2010). Challenges and recent advances in IR-UWB system design, *Proceedings of 2010 IEEE International Symposium on Circuits and Systems (ISCAS)*, pp. 3288–3291.
- [20] **Zhang, P., Hu, Z., Qiu, R. C. and Sadler, B. M.** (2009). A compressed sensing based ultra-wideband communication system, *IEEE International Conference on Communications (ICC)*, pp. 1–5.
- [21] **Novakov, E. and Fournier, J. M.** (2009). An ultra-wideband impulse-radio communication method and transceiver, *IEEE Global Telecommunications Conference (GLOBECOM)*, pp. 1–5.
- [22] **Oka, A. and Lampe, L.** (2009). A compressed sensing receiver for UWB impulse radio in bursty applications like wireless sensor networks, *Journal of Physical Communication*, **2(4)**, 248–264.
- [23] **Bajwa, W. U., Haupt, J., Sayeed, A. M. and Nowak, R.** (2010). Compressed channel sensing: a new approach to estimating sparse multipath channels, *Proceedings of the IEEE*, **98(6)**, 1058–1076.

- [24] **Berger, C. R., Wang, Z., Huang, J. and Zhou, S.** (2010). Application of compressive sensing to sparse channel estimation, *IEEE Communications Magazine*, **48(11)**, 164–174.
- [25] **Parades, J., Arce, G. R. and Wang, Z.** (2007). Ultra-wideband compressed sensing: channel estimation, *IEEE Journal on Selected Topics in Signal Processing*, **1**, 383–395.
- [26] **Yu, H. and Guo, S.** (2007). Pre-filtering ultra-wideband channel estimation based on compressed sensing, *International Conference on Communications and Mobile Computing (CMC)*, pp. 110–114.
- [27] **Barbieri, A., Pancaldi, F. and Vitetta, G. M.** (2011). Compressed channel estimation and data detection algorithms for IR-UWB, *IEEE International Conference on Ultra-Wideband (ICUWB)*, pp. 360–364.
- [28] **Başaran, M., Erküçük, S. and Çırpan, H. A.** (2011). The effect of channel models on compressed sensing based UWB channel estimation, *IEEE International Conference on Ultra-Wideband (ICUWB)*, pp. 375–379.
- [29] **Tipping, M. E. and Faul, A. C.** (2003). Fast marginal likelihood maximization for sparse Bayesian models, *Proceedings of the 9th International Workshop on Artificial Intelligence and Statistics*.
- [30] **Ji, S., Xue, Y. and Carin, L.** (2008). Bayesian compressive sensing, *IEEE Transactions on Signal Processing*, **56(6)**, 2346–2355.
- [31] **Babacan, S. D., Molina, R. and Katsaggelos, A. K.** (2009). Fast Bayesian compressive sensing using Laplace priors, *IEEE International Conference on Acoustics, Speech and Signal Processing (ICASSP)*, pp. 2873–2876.
- [32] **Yang, D., Li, H. and Peterson, G. D.** (2011). Decentralized turbo Bayesian compressed sensing with application to UWB systems, *EURASIP Journal on Advances in Signal Processing*, **2011**, article ID 817947.
- [33] **Tang, L., Zhou, Z. and Shi, L.** (2011). Ultra-wideband channel estimation based on distributed Bayesian compressive sensing, *International Journal of Digital Content Technology and its Applications (JDCTA)*, **5(2)**, 1–8.
- [34] **Shi, L., Zhou, Z., Tang, L. and Yao, H.** (2010). Ultra-wideband channel estimation based on Bayesian compressive sensing, *Proceedings of the 10th International Symposium on Communications and Information Technologies (ISCIT)*, pp. 779–782.
- [35] **Zayyani, H., Babaie-Zadeh, M. and Jutten, C.** (2009). Compressed sensing block MAP-LMS adaptive filter for sparse channel estimation and a Bayesian Cramér-Rao bound, *IEEE International Workshop on Machine Learning and Signal Processing (MLSP)*, pp. 1–6.
- [36] **Kay, S. M.** (1993). *Fundamentals of Statistical Signal Processing: Estimation Theory*, Upper Saddle River, New Jersey, Prentice Hall.

- [37] **Eldar, Y. C.** (2006). Uniformly improving the Cramér-Rao bound and maximum likelihood estimation, *IEEE Transactions on Signal Processing*, **54(8)**, 2943–2956.
- [38] **Di Benedetto, M. G., et al.** (2006). UWB Communications Systems: A Comprehensive Overview, EURASIP Series on Signal Processing and Communications, New York, Hindawi Publishing.
- [39] **Federal Communications Commission (FCC)** (2002). Revision of Part 15 of the commission’s rules regarding ultra-wideband transmission systems, first report and order, ET-Docket 98-153, FCC 02-48, Washington, DC.
- [40] **Hongson, S., et al.** (2003). On the spectral and power requirements for UWB transmission, *IEEE International Conference on Communications (ICC)*, pp. 738–742.
- [41] **Siriwongpairat, W. P. and Ray Liu, K. J.** (2005). Ultra-Wideband Communications Systems: Multiband OFDM Approach, Hoboken, New Jersey, Wiley.
- [42] **Nikookar, H. and Prasad, R.** (2009). Introduction to Ultra Wideband for Wireless Communications, Milton Keynes, UK, Springer.
- [43] **Erkücüük, S., Kim, D. I. and Kwak, K. S.** (2007). Effects of channel models and Rake receiving process on UWB-IR system performance, *IEEE International Conference on Communications (ICC)*, pp. 4896–4901.
- [44] **Molisch, A. F., et al.** (2006). A comprehensive standardized model for ultrawideband propagation channels, *IEEE Transactions on Antennas and Propagation*, **54**, 3151–3166.
- [45] **Candès, E. J. and Wakin, M. B.** (2008). An introduction to compressive sampling, *IEEE Signal Processing Magazine*, **25**, 21–30.
- [46] **Tropp, J. A.** (2006). Just relax: convex programming methods for identifying sparse signals in noise, *IEEE Transactions on Information Theory*, **52(3)**, 1030–1051.
- [47] **Donoho, D. L.** (2006). For most large underdetermined systems of linear equations the minimal ℓ_1 -norm solution is also the sparsest solution, *Journal of Communications on Pure and Applied Mathematics*, **59(6)**, 797–829.
- [48] **Candès, E. J., Romberg, J. K. and Tao, T.** (2006). Stable signal recovery from incomplete and inaccurate measurements, *Journal of Communications on Pure and Applied Mathematics*, **59(8)**, 1207–1223.
- [49] **SAS Institute Inc.** (2008). Introduction to Bayesian analysis procedures, *SAS / STAT 9.2 User’s Guide*, pp. 141–175. Date retrieved: 02.12.2012, adress: <http://support.sas.com/documentation/cdl/en/statugbayesian/61755/PDF/default/statugbayesian.pdf>
- [50] **Gelman, A., Carlin, J. B., Stern, H. S. and Rubin, D. B.** (2003). Bayesian Data Analysis, 2nd edition, Boca Raton, Florida, CRC Press.

- [51] **Berger, J. O.** (1985). *Statistical Decision Theory and Bayesian Analysis*, 2nd edition, New York, NJ, Springer.
- [52] **Bishop, C. M.** (2006). *Pattern Recognition and Machine Learning*, New York, NJ, Springer.
- [53] **Van Trees, H. L.** (1968). *Detection, Estimation and Modulation Theory (Part I)*, New York, Wiley.
- [54] **Baraniuk, R. G.** (2007). Compressive sensing, *IEEE Signal Processing Magazine*, **24(4)**, 118–121.
- [55] **Qiu, R. C. and Lu, I-T.** (1996). Wideband wireless multipath channel modeling with path frequency dependence, *IEEE International Conference on Communications*, **5(2)**, 23–27.
- [56] **Qiu, R. C. and Lu, I-T.** (1999). Multipath resolving with frequency dependence for wide-band wireless channel modeling, *IEEE Transactions on Vehicular Technology*, **48(1)**, 273–285.
- [57] **Chong, C. C., Kim, Y. E., Yong, S. K. and Lee, S. S.** (2005). Statistical characterization of the UWB propagation channel in indoor residential environment, *Journal of Wireless Communications and Mobile Computing*, **5(5)**, 503–512.
- [58] **Molisch, A. F., et al.** (2005). IEEE 802.15.4a channel model - final report, Technical Report Document IEEE 802.15-04-0662-02-004a, 2005.
- [59] **Saleh, A. A. M. and Valenzuela, R.** (1987). A statistical model for indoor multipath propagation, *IEEE Journal on Selected Areas in Communications*, **5(2)**, 128–137.
- [60] **Chong, C. C. and Yong, S. K.** (2005). A generic statistical-based UWB channel model for high rise apartments, *IEEE Transactions on Antennas and Propagation*, **53(8)**, 2389–2399.

APPENDICES

APPENDIX A: IEEE 802.15.4a UWB Channel Modeling

APPENDIX A: IEEE 802.15.4a UWB Channel Modeling

Parameters that provide the UWB channel modeling for IEEE 802.15.4a standard is presented briefly in this part of the thesis. While IEEE 802.15.4a channel models were developed within the framework of the standardization of low data rate systems, they are not only suitable for low data rate UWB systems. These channel models are valid for UWB systems regardless of their data rate and modulation form [44].

A.1 Path Gain

Path gain is defined as the ratio of the received power averaged over both the small-scale fading and the large-scale fading to the transmit power. The path gain expresses the average SNR that a system can achieve. In addition to distance dependence, due to the frequency dependence of propagation effects, it also shows dependence on frequency. Hence, distance and frequency dependent path gain is expressed as [44]

$$G(f, d) = \frac{1}{\Delta f} E \left\{ \int_{f-(\Delta f/2)}^{f+(\Delta f/2)} |H(\tilde{f}, d)|^2 d\tilde{f} \right\}, \quad (\text{A.1})$$

where $H(f, d)$ represents the transfer function from transmitter antenna connector to receiver antenna connector and the total path gain is obtained by integrating this transfer function over the whole bandwidth of interest. As mentioned above the expectation $E\{\cdot\}$ is taken over both the small-scale fading and the large scale fading. The frequency range Δf is chosen small enough so that diffraction coefficients, dielectric constants, etc., can be considered constant within that bandwidth. In order to simplify computations, distance and frequency dependent path gain can be written as a multiplication of the frequency dependence and distance dependence [44]

$$G(f, d) = G(f) G(d). \quad (\text{A.2})$$

The frequency dependence of the channel path gain is given as [55–57]

$$\sqrt{G(f)} \propto f^{-\kappa}, \quad (\text{A.3})$$

where κ represents decaying factor. The distance dependence of the path gain in dB is expressed as [44]

$$G(d) = G_0 - 10n \log_{10} \left(\frac{d}{d_0} \right), \quad (\text{A.4})$$

where d_0 is reference distance and it is set to 1m, G_0 is the measured path gain at the reference distance and n is the path gain (propagation) exponent. n depends on the environment with having either LOS or NLOS transmitter-receiver connection.

A.2 Shadowing

Shadowing (large-scale fading) gain is described as the variation of the local mean around the path gain. When the shadowing gain is taking into account, the distance dependence of the path gain in (A.4) can be rewritten as [58]

$$G(d) = G_0 - 10n \log_{10}\left(\frac{d}{d_0}\right) + S, \quad (\text{A.5})$$

where S represents the shadowing gain in dB and it is a random variable which has a Gaussian distribution with zero mean and standard deviation σ_S .

A.3 Power Delay Profile

Power delay profile describes the received signal power as a function of multipaths delay and it can be obtained using the impulse response of the channel as [42]

$$P(\tau) = E \left\{ |h(t, \tau)|^2 \right\}, \quad (\text{A.6})$$

where τ denotes the delay. The channel impulse response (in complex baseband) of the Saleh-Valenzuela (S-V) model is denoted as [44]

$$h_{discrete}(t) = \sum_{l=0}^L \sum_{k=0}^K a_{k,l} \exp(j\phi_{k,l}) \delta(t - T_l - \tau_{k,l}), \quad (\text{A.7})$$

where $a_{k,l}$ and $\phi_{k,l}$ represents the tap weight and phase of the k th component in the l th cluster, T_l is the delay of the l th cluster and $\tau_{k,l}$ is the delay of the k th multipath component relative to the l th cluster arrival time T_l . The phases $\phi_{k,l}$ are uniformly distributed, i.e., for a bandpass system, the phase is taken as a uniformly distributed random variable from the range $[0, 2\pi]$.

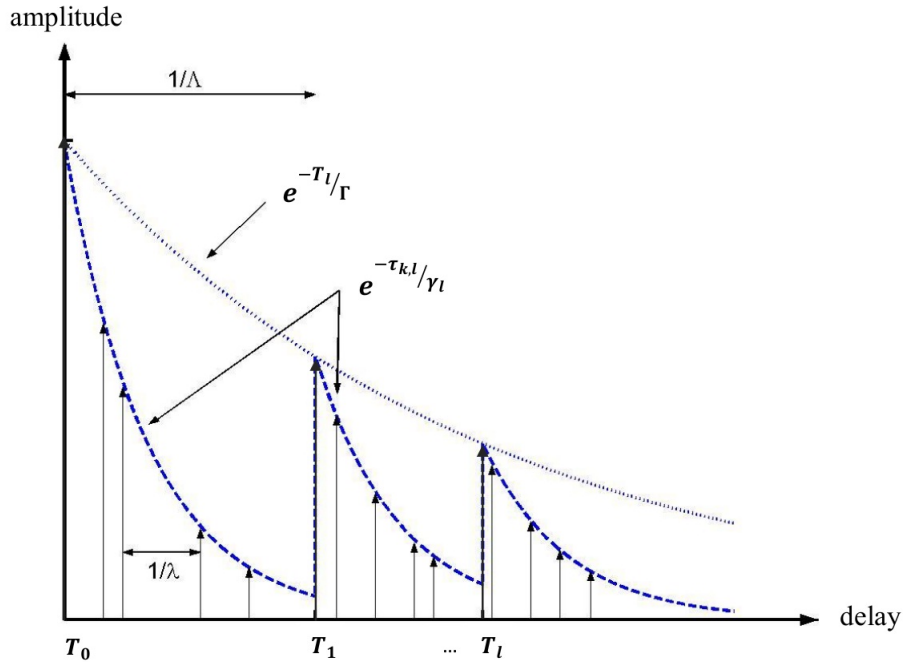


Figure A.1 : Principle of the Saleh-Valenzuela channel fading model [59].

In S-V model the strength of the clusters decreases exponentially with time and therefore there is no need to consider all clusters. The number of clusters (L) is modeled as a random variable with Poisson distribution [44]

$$pdf_L(L) = \frac{(\bar{L})^L \exp(-\bar{L})}{L!} \quad (\text{A.8})$$

so that the mean \bar{L} completely characterizes the distribution.

The distributions of cluster arrival times are modeled by a Poisson process so that the inter-cluster arrival times are exponentially distributed

$$p(T_l|T_{l-1}) = \Lambda_l \exp[-\Lambda_l(T_l - T_{l-1})] \quad l > 0, \quad (\text{A.9})$$

where Λ_l is the cluster arrival rate (assumed to be independent of l). The ray arrival times are modeled with a mixture of two Poisson process as follows [60]:

$$p(\tau_{k,l}|\tau_{(k-1),l}) = \beta \lambda_1 \exp[-\lambda_1(\tau_{k,l} - \tau_{(k-1),l})] + (1 - \beta) \lambda_2 \exp[-\lambda_2(\tau_{k,l} - \tau_{(k-1),l})] \quad k > 0, \quad (\text{A.10})$$

where β and λ_1, λ_2 represent the mixture probability and the ray arrival rates, respectively.

For some environments which have dense arrival of the multipaths such as industrial environment (CM-8), each resolvable delay bin contains significant energy. In this situation, the notion of arrival rates losses its meaning and a tapped delay line model with regular tap spacing based impulse response realization is used.

The power delay profile (the mean power of different paths) is exponential within each cluster [58]

$$E\{|a_{k,l}|^2\} = \Omega_l \frac{1}{\gamma_l [(1 - \beta)\lambda_1 + \beta\lambda_2 + 1]} \exp(-\tau_{k,l}/\gamma_l), \quad (\text{A.11})$$

where Ω_l represents the integrated energy of the l th cluster and γ_l represents the intra-cluster decay time constant.

The cluster decay time depends linearly on the cluster arrival time as [44]

$$\gamma_l = k_\gamma T_l + \gamma_0, \quad (\text{A.12})$$

where k_γ is the increase of the decay constant with delay.

The energy of the l th cluster which is averaged over both the small-scale fading and the cluster shadowing and also normalized to γ_l , follows an exponential decay in general as [44]

$$10 \log(\Omega_l) \propto 10 \log(\exp(-T_l/\Gamma)) + M_{cluster}, \quad (\text{A.13})$$

where $M_{cluster}$ is a Gaussian distributed variable with standard deviation $\sigma_{cluster}$.

For the NLOS case of some scenarios such as office and industrial, the model of the power delay profile can be different and expressed as [58]

$$E\{|a_{k,l}|^2\} = \left(1 - \chi \exp\left(\frac{-\tau_{k,l}}{\gamma_{rise}}\right)\right) \exp\left(\frac{-\tau_{k,l}}{\gamma_l}\right) \left(\frac{\gamma_l + \gamma_{rise}}{\gamma_l} \frac{\Omega_l}{\gamma_l + \gamma_{rise}(1 - \chi)}\right) \quad (\text{A.14})$$

on a log-linear scale where χ is the attenuation of the first component, γ_{rise} describes how fast the power delay profile increases to its local maximum, and γ_1 represents the decay at later times.

A.4 Small-Scale Fading

Small scale fading is defined as the instantaneous fluctuations of the received signal strength over short distances or duration times. The distribution of the small-scale amplitudes $|a_{k,l}|$ in the model expressed as Nakagami distribution [44]

$$pdf(x) = \frac{2}{\Gamma(m)} \left(\frac{m}{\Omega}\right)^m x^{2m-1} \exp\left(-\frac{m}{\Omega}x^2\right), \quad (\text{A.15})$$

where $\Gamma(m)$, $m \geq 1/2$ and Ω denote the gamma function, Nakagami- m factor and the mean-square value of the amplitude, respectively. The parameter Ω corresponds to the mean power, and hence its delay dependence is given by the power delay profile above. The m -parameter is random variable which has a lognormal distribution, whose logarithm has a mean μ_m and standard deviation σ_m . Both of the mean and the standard deviation can have a delay dependence and they are expressed as [44]

$$\mu_m(\tau) = m_0 - k_m \tau, \quad (\text{A.16})$$

$$\sigma_m(\tau) = \hat{m}_0 - \hat{k}_m \tau. \quad (\text{A.17})$$

The Nakagami- m factor is modeled differently for the first component of each cluster. It is assumed to be deterministic and independent of delay [44]

$$m = \tilde{m}_0. \quad (\text{A.18})$$

After presenting the parameters that provide the UWB channel modeling, measurement values of these channel parameters are given in Table A.2 for CM-1, CM-2, CM-5 and CM-8, respectively.

Table A.1 : Definitions of the channel parameters given in Table A.2.

| | |
|------------------------|---|
| d | transmission distance |
| G_0 | path gain at the reference distance |
| n | path gain exponent |
| S | shadowing gain |
| σ_S | standart deviation of the shadowing gain |
| κ | frequency dependence of decaying factor |
| \bar{L} | mean number of clusters |
| Λ | inter-cluster arrival rate |
| λ_1, λ_2 | ray arrival rates |
| β | mixture probability |
| Γ | inter-cluster decay constant |
| k_γ | increase of the decay constant with delay |
| γ_0 | intra-cluster decay time constant |
| $\sigma_{cluster}$ | standart deviation of cluster shadowing |
| χ | attenuation of the first path |
| γ_{rise} | describes how fast the power delay profile increases to its local maximum |
| γ_1 | decay at later times |
| m_0, k_m | Nakagami- m factor mean |
| \hat{m}_0, \hat{k}_m | Nakagami- m factor variance |
| \tilde{m}_0 | Nakagami- m factor for strong multipath components |

Table A.2 : Parameters of the IEEE 802.15.4a UWB channel models used in this thesis [44].

| Channel Parameters | CM-1 | CM-2 | CM-5 | CM-8 |
|-------------------------------|------------|------------|------------|----------|
| <i>valid range of d</i> | 7-20 m | 7-20 m | 5-17 m | 2-8 m |
| <i>frequency range</i> | 3-10 GHz | 3-10 GHz | 3-6 GHz | 3-10 GHz |
| <i>Path gain</i> | | | | |
| G_0 [dB] | -43.9 | -48.7 | -45.6 | -56.7 |
| n | 1.79 | 4.58 | 1.76 | 2.15 |
| S [dB] | 2.22 | 3.51 | | |
| σ_S [dB] | | | 0.83 | 6 |
| κ [dB/octave] | 1.12 | 1.53 | 0.12 | -1.427 |
| <i>Power delay profile</i> | | | | |
| \bar{L} | 3 | 3.5 | 13.6 | 1 |
| Λ [1/ns] | 0.047 | 0.12 | 0.0048 | |
| λ_1, λ_2 [1/ns] | 1.54, 0.15 | 1.77, 0.15 | 0.27, 2.41 | |
| β | 0.095 | 0.045 | 0.0078 | |
| Γ [ns] | 22.61 | 26.27 | 31.7 | |
| k_γ | 0 | 0 | 0 | |
| γ_0 [ns] | 12.53 | 17.5 | 3.7 | |
| $\sigma_{cluster}$ [dB] | 2.75 | 2.93 | 3 | |
| χ | | | | 1 |
| γ_{rise} [ns] | | | | 17.35 |
| γ_1 [ns] | | | | 85.36 |
| <i>Small-scale fading</i> | | | | |
| m_0 [dB] | 0.67 | 0.69 | 0.77 | 0.36 |
| k_m | 0 | 0 | 0 | 0 |
| \hat{m}_0 [dB] | 0.28 | 0.32 | 0.78 | 1.15 |
| \hat{k}_m | 0 | 0 | 0 | 0 |
| \tilde{m}_0 | | | | |

CURRICULUM VITAE



Name Surname: Mehmet ÖZGÖR

Place and Date of Birth: Ankara / Turkey - July 21, 1988

E-Mail: mehmetozgor@ieee.org

B.Sc.: 2006 - 2010, Dept. of Electrical and Electronics Engineering
Karadeniz Technical University

2008 - 2012, Dept. of Business Administration
Anadolu University

Professional Experience and Rewards:

- | | |
|-------------------|---|
| 01/2012 - present | İstanbul Kültür University, Dept. of Electronics Engineering Research Assistant |
| 10/2010 - 01/2012 | Doğuş University, Dept. of Electronics and Communication Engineering Research Assistant |
| 10/2010 - 08/2012 | TÜBİTAK Graduate Scholarship |
| June 5, 2010 | Karadeniz Technical University 2nd place graduation award for the B.Sc. degree in both Faculty of Engineering and Dept. of Electrical and Electronics Engineering |

List of Publications:

PUBLICATIONS/PRESENTATIONS ON THE THESIS

- **Özgör M.**, Erküçük S., Çırpan H. A., 2012: Bayesian Compressive Sensing for Ultra-Wideband Channel Models. *35th International Conference on Telecommunications and Signal Processing (TSP 2012)*, July 3-4, 2012 Prague, Czech Republic.
- **Özgör M.**, Erküçük S., Çırpan H. A., 2012: Bayesian Compressive Sensing for Ultra-Wideband Channel Estimation: Algorithm and Performance Analysis, accepted for publication in *Telecommunication Systems Journal*.